Applied Catalysis B: Environmental 339 (2023) 123146

Contents lists available at ScienceDirect

Applied Catalysis B: Environmental

journal homepage: www.elsevier.com/locate/apcatb

Photo/electrochemical urea synthesis via CO_2 coupling with nitrogenous small molecules: Status and challenges for the development of mechanism and catalysts

Jili Yuan [a,*], Lin Hu [b], Jun Huang [a], Yuqing Chen [c], Shanshan Qiao [c], Haibo Xie [a,*]

[a] Department of Polymer Materials and Engineering, College of Materials & Metallurgy, Guizhou University, Huaxi District, Guiyang 550025, PR China
[b] Department of Research and Development, Huaneng Clean Energy Research Institute, Beijing 102209, PR China
[c] State Key Laboratory of Chemo/Biosensing and Chemometrics, Hunan University, Changsha 410082, PR China

ARTICLE INFO

Keywords:
Photo/electrocatalytic urea synthesis
C−N coupling pathway
CO_2RR
N_2 fixation
Nitrate reduction reaction

ABSTRACT

Urea (NH_2CONH_2) is an essential fertilizer for humanity. Nevertheless, industrial urea production and its feedstock NH_3 production are energy-extensive and involve largely carbon footprints. Currently, urea production via electro/photochemical routes have shown a significant appeal and potential because only water, environmentally CO_2 and nitrogenous small molecules, and solar energy/electricity are involved during the whole process. In the past few years, considerable efforts have been devoted to revealing the mechanism of the C−N coupling processes and the development of advanced electro/photocatalysts for the selective synthesis of urea. In this review, we compare and contrast the two distinct yet inherently closely linked catalytic C−N processes, before we detail recent advanced in the catalytic active sites construction of different urea catalyst systems from the viewpoint of electrochemical and photochemical approaches. We close with a balanced outlook on the current challenges and promising opportunities.

1. Introduction

Urea (NH_2CONH_2) was firstly artificially synthesized using two inorganic molecules as feedstocks from Friedrich Wöhler in 1828 [1]. A breakthrough is through pyrolyzing ammonium carbamide to urea in 40 years latter [2]. Subsequently, industrial urea production (Bosch-Meiser process) was first developed in 1922 [3]. This pathway involves two steps: (i) liquid ammonia (NH_3) reacts with carbon dioxide (CO_2) to form ammonium carbamate ($CH_6N_2O_2$) and (ii) this compound further decomposes into urea and water. Benefiting from the high nitrogen content (46%) of urea and readily releasing NH_3 into the soil, urea has gradually become the most used nitrogen fertilizer on the earth [4]. And the application fields of urea are further enlarged, such as fertilizer on Mars, urea-based resins, urea-containing creams, animal feed, barbiturates, and cleaning additives [5–8]. Therefore, the mass industrial production of urea is of great significance for the development of human civilization. Unfortunately, the Bosch-Meiser process not only runs under around 150 bar of high pressure and above 180 °C of elevated temperature, but also produces vast quantities of CO_2 and consumes large fossil fuels [9,10]. Specifically, per ton of urea production consumes 21 − 29 billion million kilojoules of energy and releases 0.7 − 2.3 tons of CO_2 emission on average [11,12]. Moreover, the feedstock NH_3 production relies on the Habor-Bosch process of more demanding conditions and the ensuing large amounts of fossil fuel consumption and CO_2 emissions [13]. Therefore, it is greatly attractive to develop a green and sustainable urea production technology for energy-saving and zero-carbon footprint, directly using naturally abundant CO_2 and nitrogenous species under ambient conditions.

Photocatalytic and electrocatalytic technology is driven by solar energy or renewable-energy-derived electricity, demonstrating significant potential to enable energy-saving a zero-carbon urea production via CO_2 coupling naturally abundant nitrogenous species [14–16]. In the past three decades, the green pathways of photo/electrocatalytic C−N coupling to produce organonitrogen compounds have been developed via co-reduction of CO_2 and nitrogenous species (such as NO_3^-, NO_2^-, NH_3, N_2, and NO), such as amide, urea, and amine products [14]. However, there is largely distinguishing difference between the formation pathway of urea and other amine organics products, particularly, the pathway of the C−N coupling process and the valence state unchangeableness of C atom from CO_2 conversion to urea. Thereby it is

* Corresponding authors.
E-mail addresses: jlyuan@gzu.edu.cn (J. Yuan), hbxie@gzu.edu.cn (H. Xie).

https://doi.org/10.1016/j.apcatb.2023.123146
Received 13 June 2023; Received in revised form 27 July 2023; Accepted 1 August 2023
Available online 2 August 2023

essential to understand the formation pathway of the photo/-electrocatalytic C−N coupling to selectively form urea. At the early stage, several carbon and nitrogen sources were used to reveal the key intermediates of the C−N coupling for urea synthesis via the control experiments, such as, CO_2, CO, and HCOOH for carbon species, N_2, NH_3, NO_3^-, NO, and NO_2^- for nitrogen species [11,17,18]. In recent years, there are several green C−N coupling pathways proposed through electrocatalytic technology [19]. Unfortunately, it is rare to reveal the mechanism of photocatalytic C−N coupling to form urea [11], possibly because the C−N coupling to form urea over photocatalysts require the three fundamental steps and their mutual collaboration, including improving light adsorption, tuning band structure, accelerating charge separation and migration, and enhancing surface photocatalytic reaction selectivity [20–23]. Thereby there is a challenge for the development of the photocatalysts due to these comprehensive requirements, causing that the TiO_2-based photocatalyst dominates currently for photocatalytic urea synthesis [16]. But for the pathway of urea electrosynthesis, substantial efforts have recently been devoted to electrocatalytic CO_2 coupling with naturally abundant nitrogen sources to synthesize urea [24–29]. Currently, a variety of electrocatalysts has been developed via various strategies, including construction various heterostructures, single/dual-atom sites, defects and doping engineering, and so on [24–30]. But the key challenge is still from the lack of efficient electrocatalysts because of the difficulty in balancing the co-activation of carbon and nitrogen sources and the subsequent catalytic C−N coupling of in situ generated species [24,25]. Although the green pathways of urea synthesis stay at the different stage, there are some mutual regulations deserved to attention. From the thermodynamics perspective of green urea synthesis, the urea formation reaction via using CO_2 and nitrogenous species (NO_3^-, NO_2^-, NH_3, N_2, and NO) as reactants is exothermic. From the kinetic perspective, the chemical inertness of N_2 ($N{\equiv}N$, 941 kJ mol^{-1}) is slightly different to CO_2 ($C{=}O$, 806 kJ mol^{-1}) [31,32]. There is the huge difference between CO_2 and nitrogen oxide (NO, NO_3^-, and NO_2^-, N − O, 204 kJ mol^{-1}) [33–37], and the CO_2, N_2 and NO as reactants are gas state, which the formation of gas-liquid-solid interface at photo/electrocatalytic C−N coupling process. Therefore, there are sluggishly kinetic processes at catalytic interface in photo/electrocatalytic processes, which even aggravates the difficulty for designing and constructing the active sites structure over photo/electrocatalysts [38–41]. Photo/electrocatalytic urea synthesis involves multistep chemical processes (including the proton coupling electron transfer process, PCET) and chemical steps (C−N coupling) [24]. Besides, the competition reactions, including hydrogen evolution reaction (HER), the parallel CO_2 reduction reaction (CO_2RR) and nitrogen reduction reaction (NRR including N_2RR/NO_3^-RR/NO_2^-RR/-NORR) cause the lower selectivity of the urea formation via the C−N coupling pathway. Although the other high value-added products can simultaneously be produced, the complex products enhance the separation cost. Therefore, it is currently necessary to overall analyze the difference between carbon and nitrogen reactants and understand the C−N coupling steps to guide the construction of the active sites over catalysts, eventually to improve the selectivity and activity of green urea synthesis pathways.

This review mainly focuses on the status and challenges for green urea pathways via photo/electrocatalytic technology (Fig. 1). Primarily, the reaction pathways of green urea synthesis are classified into two kinds of processes due to the chemical inertness difference between carbon and nitrogen reactants, and the corresponding competition reactions are summarized systematically. Then, the formation pathways of urea were comprehensively summarized at the catalytic interface, mainly including the C−N coupling process of in situ generated species, the adsorption of reactants, proton coupling electron transfer (PCET), and desorption of species. Subsequently, the development of photo/electrocatalysts and their structural feature are elaborated logically. Finally, the future challenges of urea photo/electrosynthesis are proposed. The review aims to provide a guide for the systematic design and construction of photo/electrocatalysts and boost industrial photo/electrocatalytic urea production.

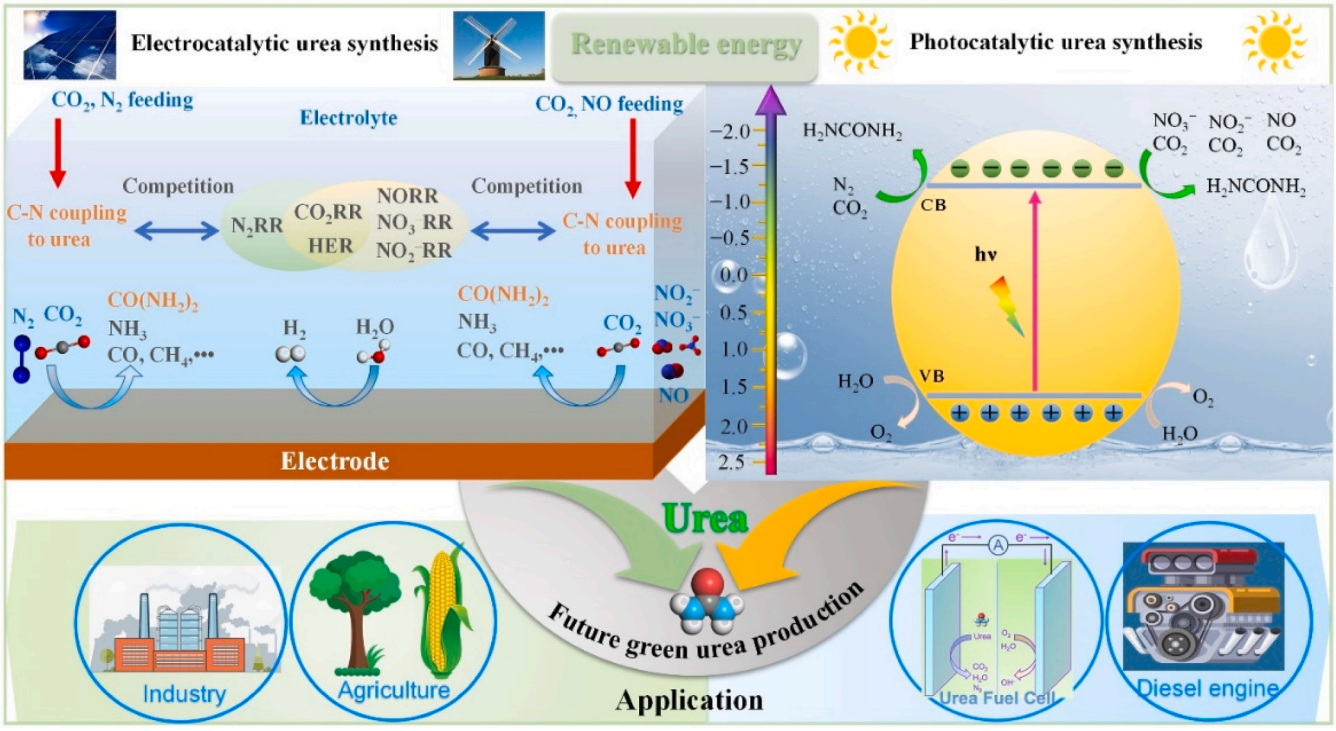

Fig. 1. An illustration of green urea synthesis technologies, including photocatalytic and electrocatalytic urea synthesis. Commercially, urea can be used as agricultural fertilizers, industrial feedstocks, energy carriers for vehicles, and urea fuel cells.

2. Proposed reactions pathway for green urea synthesis

Photo/electrocatalytic urea synthesis is generally a multi-step reaction that can proceed through the competing of the C−N bond formation and the parallel self-reduction reaction of where CO_2, H_2O, and naturally abundant nitrogen-containing compounds N_2, NO, NO_2^-, and NO_3^- are used as the carbon, hydrogen, and nitrogen sources, respectively. Owing to the chemical inertness difference between CO_2 and nitrogen reactants, they are classified into two types, N≡N and N − O. As schematically shown in Fig. 1, the main reaction pathways of urea photo/electrosynthesis are as below (Eqs. (1)–(4)). The standard reduction potential (pH 0) versus standard hydrogen electrode (SHE) is shown on the right.

$$CO_2 + N_2 + 6\,H^+ + 6e^- \rightarrow NH_2CONH_2 + H_2O\ E^o = 0{\cdot}211\ V \quad (1)$$

$$CO_2 + 2\,NO + 10\,H^+ + 10\,e^- \rightarrow NH_2CONH_2 + 3\,H_2O\ E^o = 0{\cdot}772\ V \quad (2)$$

$$CO_2 + 2NO_2^- + 16\,H^+ + 14e^- \rightarrow NH_2CONH_2 + 5\,H_2O\ E^o = 0{\cdot}833\ V \quad (3)$$

$$CO_2 + 2NO_3^- + 18\,H^+ + 16e^- \rightarrow NH_2CONH_2 + 7\,H_2O\ E^o = 0{\cdot}811\ V \quad (4)$$

The main competition reactions are as follows (Eq. (5); CO_2 reduction potential, Eq. (6); the competing proton reduction potential, Eqs. (7)–(10): $N_2/NO_2^-/NO_3^-/NO$ reduction potential):

$$CO_2 + 2\,H^+ + 2e^- \rightarrow CO\ (g) + H_2O\ E^o = -0{\cdot}106\ V \quad (5)$$

$$2\,H^+ + 2e^- \rightarrow H_2\ E^o = 0\ V \quad (6)$$

$$N_2\ (g) + 8\,H^+ + 6e^- \rightarrow 2\,NH_4^+\ E^o = 0{\cdot}275\ V \quad (7)$$

$$NO\ (g) + 6\,H^+ + 5e^- \rightarrow NH_4^+ + H_2O\ E^o = 0{\cdot}836\ V \quad (8)$$

$$NO_2^- + 8\,H^+ + 6e^- \rightarrow NH_4^+ + 2\,H_2O\ E^o = 0{\cdot}897\ V \quad (9)$$

$$NO_3^- + 9\,H^+ + 8e^- \rightarrow NH_4^+ + 3\,H_2O\ E^o = 0{\cdot}875\ V \quad (10)$$

For possible parallel competition reactions, the standard reduction potential (pH 0) versus standard hydrogen electrode (SHE) is shown on the right [42,43]. From the thermodynamical perspective, based on these standard reduction potentials of carbon and nitrogen parallel reactions, the urea synthesis pathways via $N_2/NO/NO_2^-/NO_3^-$ coupling with CO_2 can proceed at the positive reduction potential (pH 0), which is thermodynamically feasible for urea formation, particularly, the urea synthesis pathway from CO_2 and N_2 co-reduction show a low positive potential. From the kinetic perspective, the urea synthesis pathway for $NO/NO_2^-/NO_3^-$ as nitrogen reactant require two times the C−N coupling processes rather than one time via the formation of key intermediate *NCON* from CO_2 and N_2. Besides, more publications reported the feasibility of the pathway for photo/electrocatalytic CO_2 coupling $NO_2^-/NO_3^-/NO$ to form urea require a relative low potential compared to the pathway of CO_2 coupling with N_2 [44–48]. Thus, we can conclude that the pathway of urea synthesis from CO_2 and N_2 co-reduction has a huge challenge compared to other pathways, particularly, the co-activation of the carbon and nitrogen reactants and the formation of key intermediate *NCON* . As for the pathways of urea synthesis via CO_2 coupling with $NO/NO_2^-/NO_3^-$, there is a huge difference of the activation energy for carbon and nitrogen reactants need to balance the rate of the stimulating reactants with respective to the stoichiometric ratio, which is attributed that there are at least three kinds of competition reactions inevitably happening for each urea synthesis pathway such as HER, CO_2RR and NRR [31–37].

Meeting to the above challenges for the green urea synthesis via these routes, it is currently vital to disclose the development principle of catalyst. Generally, the entire process of urea photo/electrosynthesis need to deeply monitor and reveal the selective urea formation of key steps, such as the adsorption way for the reactants at catalytic site and the C−N coupling process [49]. Currently, thereby the advanced in situ/operando characterizations and theoretical simulations have been used to unveil reactant intermediates, the dynamic structures of catalysts, catalytic active species, reactive intermediates, and the reaction pathway of urea synthesis [19]. These in-depth analyses can build up the key descriptor of the C−N coupling steps for each urea formation pathway, facilitating the rational design and construction of an effective catalyst, thereby accelerating the development of the catalyst construction methodologies, eventually realizing highly selective the C−N coupling to produce urea for each pathway (Fig. 2).

At the current stage, the investigation of urea formation mechanism from N_2 or $NO_2^-/NO_3^-/NO$ and CO_2 co-reduction is still underexplored. Fortunately, five kinds of the C−N coupling pathway have been revealed indirectly or directly by in situ characterization techniques and DFT calculations, including the key intermediate of *NCON, *$CONH_2$, *$CONO_2$, *CONO, and *CONH as the descriptor for urea formation. Besides, the key descriptor formation can be adjusted by the structure feature of active site over catalyst, thereby it can guide direction for the construction strategy of active site over catalyst. For examples, introducing the large amount of oxygen vacancy over catalyst is selective to the formation of the key intermediate*OCNO and constructing the dual atom sites over catalyst is selective to the formation of the key intermediate *CONH rather than the other four kinds of the key intermediate for the C−N coupling pathway [19]. Therefore, as schematically illustrated in Fig. 2, we proposed more kinds of the C−N coupling pathway to form the key intermediate, including *$HOOCNH_2$, *$OOCNH_2$, *NCON, *$CONH_2$, *$CONO_2$, *CONO, and *CONH.

2.1. Proposed mechanisms for urea photo/electrosynthesis

In view of that the four kinds of pathways of the photo/electrocatalytic urea synthesis should be spontaneous thermodynamically, thereby the kinetic process of these routes, mainly including the activation and adsorption of reactants, PCET, and the C−N coupling process, has been much attentions [19,48,49]. Each pathway for urea photo/-electrosynthesis corresponds to the different nitrogen sources, resulting in the mechanism difference for the kinetic process of urea synthesis. The pathway of the CO_2 coupling with N_2 happens to three main challenges: i) the arduous activation of inert N_2/CO_2 molecule on the catalysts surface [50], ii) the high energy barrier of the N≡N and C═O bond dissociation [51,52], and iii) the hindrance of the desired C−N bond coupling reaction by the inevitable competitive N_2RR, HER and CO_2RR, and thus further lowering urea electrosynthesis selectivity with the distribution of the complex products [44,46,53,54]. For the coupling CO_2 with nitrogen alternatives (NO_3^-, NO_2^-, and NO) pathway, although these alternatives are easily to be activated, the huge difference in activation energy between C═O (806 kJ mol^{-1}) and N − O (204 kJ mol^{-1}) also results in a much faster rate of NO_3^-RR/NO_2^-RR than that of CO_2RR, which readily makes the competitive NRR reaction dominate to hinder the C-N coupling. There is a significant challenge how to balance the activation efficiency of reactants and enhance selective the C−N coupling to form urea.

The mechanism of photochemical and electrochemical urea synthesis has also some different point due to the moderate photocatalytic process. Three phases make up the usual photocatalytic process [55–57] (Fig. 3): light absorption by the light-absorbing material in photocatalyst; (2) separation and migration of the photogenerated charge carriers; (3) surface redox reactions with the assistance of cocatalysts on the semiconductor surface. Additionally, the process of charge carrier migration is always accompanied by carrier recombination, including surface and bulk recombination, neither of which are conducive to photocatalysis and should be avoided as much as possible. First of all, the occurrence of urea photosynthesis reaction needs to meet thermodynamics requirements [58,59] (Fig. 3): The incident photon energy must be at least equal to the optical bandgap (Eg) of the semiconductor, (2) the semiconductor's valence band maximum must be more positive than the donor's oxidation potential ($E_{(D/D\cdot)}$), and (3) the conduction band minimum must be more negative than the acceptor's reduction

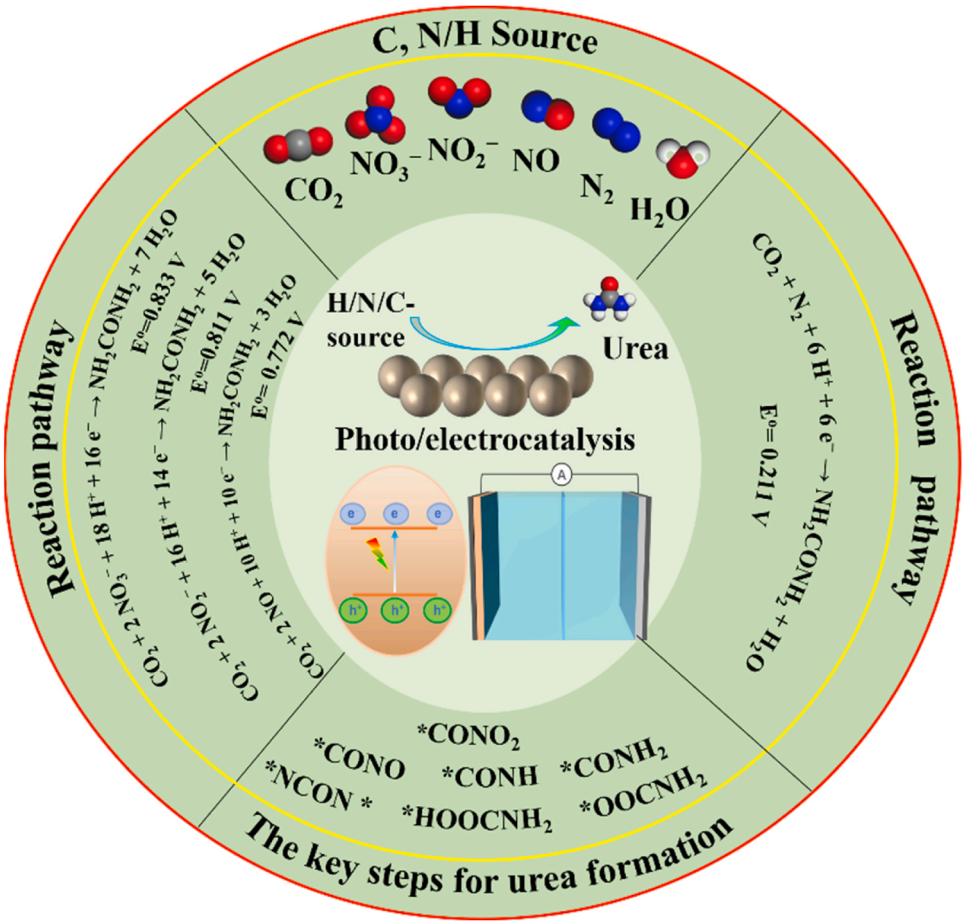

Fig. 2. Schematic illustration of photo/electrosynthesis of urea: carbon, nitrogen, and hydrogen source, the C–N coupling reaction pathways and the corresponding thermodynamical equilibrium potential (pH 0), and the key steps of the photo/electrocatalytic C–N coupling for each reaction pathway.

potential ($E(_{A+/A})$). Based on these principles, as shown in Fig. 3, compared to the reduction potential of nitrogen small molecules, it is observed that the reaction of photocatalytic CO_2 reduction to CO needs to be larger reduction potential. From the kinetic perspective, photocatalysis also happens to several typical kinetic challenges: Firstly, the three fundamental steps—light absorption (10^{-15}–10^{-9} s), charge separation and transport (10^{-15} s), and surface reactions (10^{-3}–10^{-1} s)—have vastly different timescales. This makes it extremely difficult to maximize the three steps' synergy [60]; Secondly, there is an inherently contradictory for an energetical photocatalyst because a broaden light absorption corresponds to a narrow bandgap and a strong redox ability means large reduction and oxidation capacity; Thirdly, since semiconductor photosensitizers lack active sites, cocatalysts must often be added to the surface of the semiconductor to increase charge separation, transfer, and reduce overpotential. Moreover, the rection kinetic challenges of these pathway of urea photo/electrosynthesis should also overcome.

2.1.1. *Mechanisms insight for the pathway from N_2 and CO_2*

The kinetic steps of photo/electrochemical co-reduction of CO_2 and N_2 for urea synthesis has been firstly revealed by Wang and co-workers in 2020 [46], even though the pioneering work on urea synthesis from CO_2 and N_2 by Kõleli et al. in 2016 [61]. Wang et al. were firstly used the isotope-labeling operando synchrotron-radiation Fourier transform infrared spectroscopy (SR-FTIR) to monitor the evolution of dynamic structure at the catalytic interface, the onset potential of CO_2 and N_2 reduction show explicitly potential dependent, respectively. The stretching vibrations of NH_2 and NH were appeared at the low reduction potential, subsequently, the stretching vibration of C═O and C–O appeared at the high reduction potential, suggesting that N_2 is preferentially electro-reduced, and then CO_2 , which is agreed with the equilibrium potential of their parallel reactions (Eqs. 5–7). The possible reaction pathway was further revealed by theoretical simulations, demonstrating that CO_2 was reduced to *COOH intermediate and N_2 is firstly absorbed on adjacent metal sites by a side-on configuration (Fig. 4a) [62] Subsequently, the released CO showed a matched molecular orbital with the *N = N * , which is favorable for the formation of a tower-like urea precursor *NCON* . Subsequently, Zhu et al. summarized the possible reaction pathway from N_2 and CO_2 [63]. The entire reaction was divided into four stages (Fig. 4a): (1) the surface adsorption of N_2 and CO_2; (2) the reduction of *CO_2 to *CO; (3) the coupling of *N_2 and *CO into *NCON* ; (4) the hydrogenation of *NCON* to urea. In all, the formed *NCON species could be further reduced to urea via four PCET steps following either the distal or the alternative pathway. Therefore, CO_2 being selectively reduced to *CO and a side-on configuration of the N_2 adsorption is an important prerequisite for the formation of *NCON* (Fig. 4a). Zhu et al. discovered that the binding energy of the *OCHO species on three MBenes is higher than *COOH [63], implying that the formation of *OCHO species is thermodynamically preferred for CO_2 reduction. However, this phenomenon from theoretical simulations does not agree with the previous study [64]. Cheng et al. further revealed that the formed *COOH and *OCHO can be obtained through either accepting a proton from water (Eley-Raideal (ER) mechanism) or through accepting a surface-bound proton (Langmuir-Hinshelwood (LH) mechanism) [65]. Although these studies mainly focus on the kinetic barrier of the CO_2 reduction to *CO process, the kinetic barrier should also be considered for this kind of the side-on adsorption configuration of N_2 over catalysts. It is worthy note that the

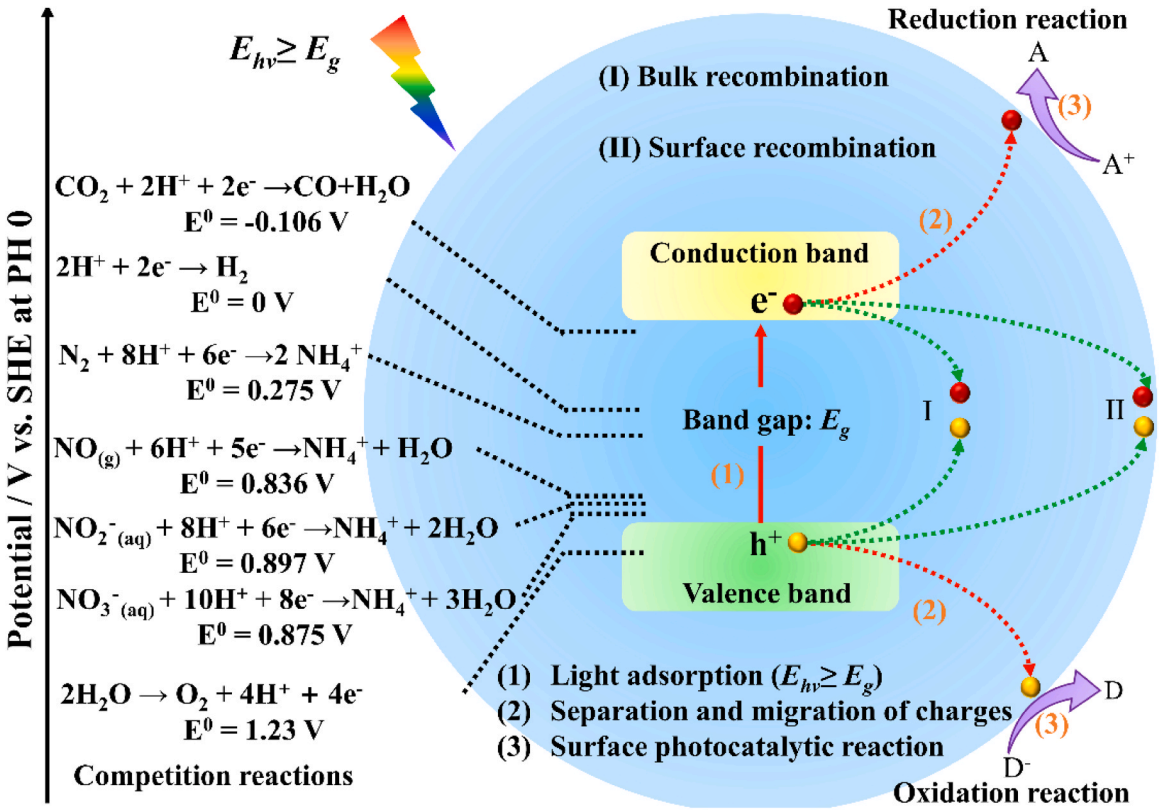

Fig. 3. Fundamentals of photocatalysis: Basic process of photocatalysis and the possible reaction equation for urea synthesis.

adsorbed *N = N * configuration did not detect by in situ characterization. Subsequently, Zhang et al. considered that the N_2 and CO_2 reactants possess different electrophilic/nucleophilic regions, constructing Mott-Schottky catalyst of Bi-$BiVO_4$ with the spontaneous charge transfer regions and promoting electrostatic interaction with carbon and nitrogen reactants, facilitating the desirable *NCON* intermediate formation [66]. Moreover, the C atom in the CO_2 molecule and the N atom ins the N_2 molecule is electron deficient and rich, respectively, theoretical simulations revealed that $BiFeO_3$/$BiVO_3$ heterostructure interreacted with the carbon and nitrogen reactants, respectively, which can facilitate the formation of *NCON* [53]. On the basis of these findings, Zhang et al. further constructed the frustrated Lewis pairs (FLPs) of $Ni_3(BO_3)_2$ as catalyst [26]. Generally, the coordinated unsaturated metal sites acted as the Lewis acid (LA), and the metal hydroxyl groups served as the Lewis bases (LB). Therefore, the LA center coupled with empty orbitals could accept the lone pair electrons of the N atom in the N_2 molecule, and the occupied π/σ orbitals of N_2 firstly donate their electrons to empty d orbitals of the LA centers, and the LB sites enriched with excess electrons could be donated to the C atom in CO_2 the electrons from the electron-rich LB sites donate to the empty σ * /π * orbital of CO_2 [67]. More importantly, the low e_g orbitals-occupied metal sites participate in the reaction, and the preferentially adsorbed *N = N * initially donate the σ orbitals to the carbine characteristic *CO, which directly couples with *N = N * through the σ orbital electron transfer to generate *NCON* urea precursors [67,68]. Besides, metal-organic frameworks (MOFs) with host-guest molecular interaction, corresponds to the desirable local electrophilic and nucleophilic regions, and the low e_g orbital occupied $Co^{4+}(t_{2g}^4 e_g^1)$ in MOFs easily accepts electrons from σ orbital of *N = N * and effectively triggers the C–N coupling reaction to emerge *NCON* urea precursor [54]. This kind of the unique σ orbital carbonylation strategy not only can improve the activation of both carbon and nitrogen reactants, but also promote the *CO and *N = N * coupling to form the *NCON* of the key intermediates.

Besides, Ghorai et al. reported that the formation of *NCON on Pyridinic-N_1 and Cu centers is through the co-reduction of N_2 to *NN and CO_2 to *CO, particularly, the adsorption configuration N_2 via end-on, and the intermediates formation of *NCON is still the key step (Fig. 4b) [69]. In all, it is regrettable that the adsorption configurations of N_2 on active site over catalyst is not consider the kinetic barrier. Moreover, in contrast to CO_2, N_2 is preferentially reduced to form the *NH_x intermediate species [44], and the *NH_x is a kind of nucleophilic agent, which means that there is possibly another descriptor for the C–N coupling pathway from N_2 and CO_2, such as *$CONH_2$ and *CONH. Subsequently, the two kinds of the key descriptor couple with *NH_2 or *NH on the adjacent active sites, rather than the prior formation of NH_x intermediate species waiting for the CO_2 firstly reduction to form *CO and further desorbed. Fortunately, Wang and co-workers have reported recently that the Zn−Mn sites with axial chloride coordination not only are favorable for the elongating N≡N via the configuration of side on instead of breaking N≡N, but also can improve the desorption of the *CO (derived from CO_2 reduction) and enable to extremely bear the CO species, thereby realizing the one-step C−N coupling process of CO species with adsorbed N_2 molecules, rather than the possible two-steps C−N coupling process from the absorbed *CO and *NH_x [70]. Therefore, this study broken through the previous cognition that urea electrosynthesis must possess ammonia synthesis activity. However, these conclusions are mainly based on the results from DFT calculations, there is no directly evidence to verify the adsorbed *N = N * formation via side-on. Moreover, it is ambiguous for the feasible pathway of the *NCON* formation whether is through that the *CO intermediates have to desorb and further attack the hypotheticals *N = N * or *N = N intermediates (Fig. 4).

Photocatalytic CO_2 coupling with N_2 to synthesize urea in an aqueous solution also involve the kinetic multi-step, including the adsorption and activation of reactants, PCET process, C−N coupling process, and hydrogenation process. Currently, Maimaiti et al. were used coal-based carbon nanotubes with the Fe-core-supported

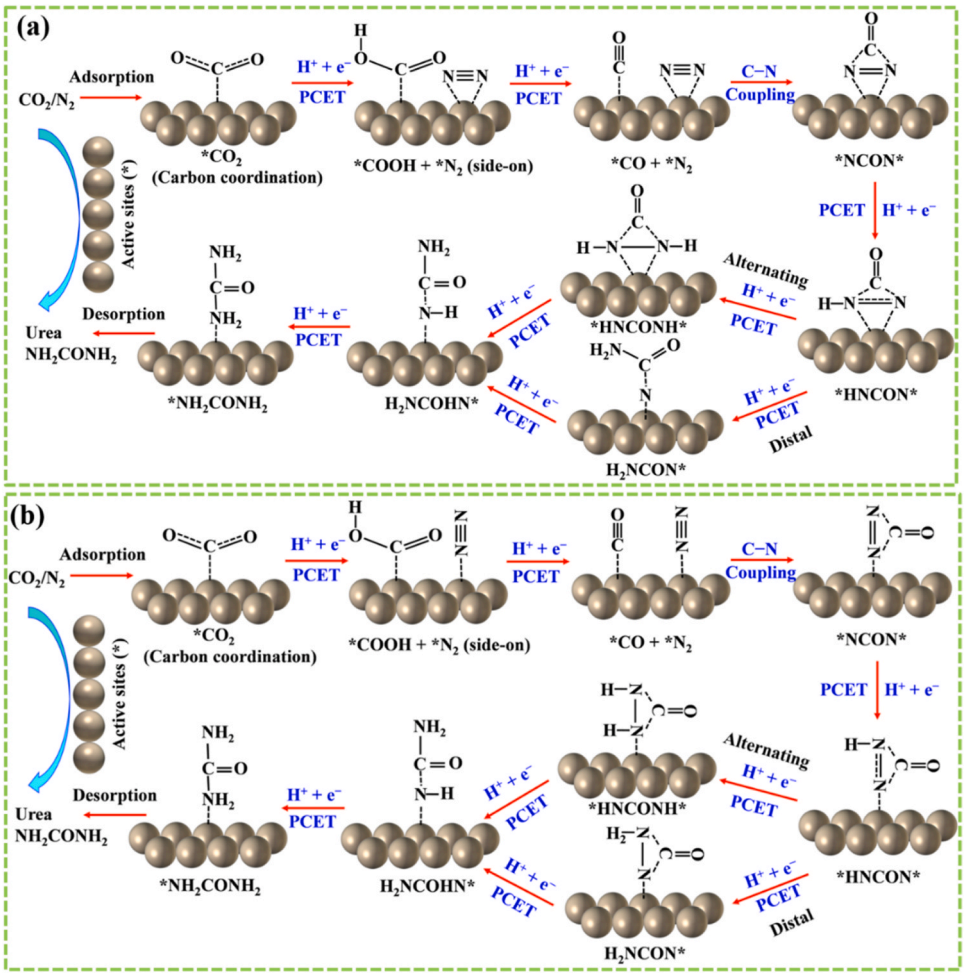

Fig. 4. Different proposed mechanisms of urea electrosynthesis from CO_2 and N_2 and their derives: the formation pathway of *CO from CO_2, the adsorption way of N_2 via (a) side-on and (b) end-on, *CO + *N_2 coupling mechanisms with different hydrogenation routes and rate determination step (RDS).

Ti^{3+}−TiO_2 composite (Ti^{3+}−TiO_2/Fe-CNTs) as photocatalyst for urea synthesis from N_2 and CO_2 [71]. The mechanism of the photocatalytic C−N coupling to form urea from N_2 and CO_2 on the surface of Ti^{3+}−TiO_2/Fe-CNTs was speculated by Maimaiti et al. The first step is optimal arrangement of the two-site catalysis of Ti^{3+} and oxygen vacancy firstly absorbed the N atoms of the N_2 molecule. The next step was N_2 hydrogenation process and breaking the C−O bond, respectively. And the last step is a formation of the C−N bond. Thus, the molecular N_2 and CO_2 converted into $CO(NH_2)_2$ via the transition of the six-membered cyclic intermediate of C and N. Although the authors were based on the analysis results of products and proposed the mechanism of the surface reaction, the proposed mechanism for urea formation is via the *CO and *NH_2 coupling on the specific arrangement structure of Ti^{3+} and oxygen vacancy [71]. Thus, this deduction may be not reasonable, but this the C−N coupling pathway is for sure. For example, the authors revealed that several kinds of the of reduction products appeared, such as, H_2, NH_3, $C_3H_6O_2$ and $C_4H_8O_2$, and several kinds of the photocatalytic oxidation reaction products produced, such as, NO_2^- and NO_3^-. Thereby the authors proposed that CO_2 molecules participated in the reduction reaction, while N_2 molecules took part in the reduction and oxidation reactions simultaneously. These results can conclude the possibility of another urea formation pathway: N_2 firstly oxidized to NO_2^-/NO_3^- and further coupling with CO_2 to form urea, which indicated that there is a huge difference between photosynthesis and electrosynthesis of urea due to the N_2 oxidation pathway. Recently, Zhang and co-worker constructed TiO_2-immobilized reversible single-atom copper (Cu SA-TiO_2) as photocatalyst to enhance the supply of efficient-electron transfer and further accelerate the co-activation of CO_2, N_2, and H_2O, eventually realizing the multi-electron-demanding urea synthesis [48]. This strategy allows the assurance of abundant and continual photogenerated electrons for multi-electron-demanding co-photoactivation of N_2 and CO_2 due to reversible single-atom copper over photocatalyst. Therefore, defect-engineering and Cu doped in TiO_2 enable to adjust the photo-absorption, accelerate charge carrier separation, and facilitate the activity of surface reaction. Recently, Liu et al. reported that the CO_2 reduction to CO is prior to the activation of N_2 on the surface of NiCoP over the flowerlike microspheres of $ZnIn_2S_{4-x}$, and the desorbed CO are further coupled with *N = N * molecules (activated N_2) to generate the urea precursor *NCON* , subsequently, the H atoms link to the N atoms leading to the formation of H_2NCONH_2 [72].

2.1.2. *Mechanism insight for the pathway from NO_3^-/NO_2^-/NO and CO_2*

At the early stage, Shibata and Furuya et al. first synthesized urea using a Cu-loaded gas diffusion electrode from CO_2 and NO_3^-/NO_2^-. Only based on the control experiment results, the authors concluded that both CO_2-derived CO-like and NO_2^--derived NH_2-like intermediates, instead of the CO and NH_3 products, are necessary to form urea [18]. Subsequently, many continued efforts from the same research group were devoted to urea electrosynthesis from CO_2 and NO_3^-/NO_2^-. Recently, based on theoretical simulations and in situ characterizations results, the pathway through the CO_2RR to *CO intermediate coupling with the NO_3^-RR/NO_2^-RR to *NH_2 intermediate to form the *$CONH_2$ intermediates is a key step for urea electrosynthesis from CO_2 and NO_3^-/NO_2^-/NO were reported by Hu et al. [73], Zhang et al. [27], Yu

et al. [25], Shao et al. [74], Zheng et al. [75], and Rose et al. [76]. Both Zhang and Yu et al. were used in situ tools to monitor the C−N coupling to produce urea process from $CO_2 + NO_2^-/NO_3^-/NO$ [25,27]. They all confirmed that the improved ability to produce $*NH_2$ and *CO intermediates could accelerate the coupling of $*NH_2$ and *CO for urea formation (Fig. 5a and b). However, Wang et al. pointed out that *CO and CO should co-exist and be interconvertible under equilibrium conditions [44]. Thus, for CO and NO_2^- co-electroreduction, the $*NH_2$ and *CO intermediates should co-exist, yet various studies verified that no urea was produced under these control conditions [74–76]. Thus, Wang et al. thought that *CO may not be species for the C−N coupling, and they also thought that the coupling process between $*NH_2$ and *CO is likely a nucleophilic attack by $*NH_2$, but compared to *CO, CO_2 is principally a better electrophile species, and is favorable to attack a nucleophilic nitrogen intermediate [44]. Even though, currently, there is no directly evidence to confirm the intermediates formation of $*CONH_2$. Therefore, the other C−N coupling to form urea pathway is further revealed.

Another C−N coupling to synthesize urea pathway, reported by Yu et al., is through the coupling process between $*CO_2$ and $*NO_2$

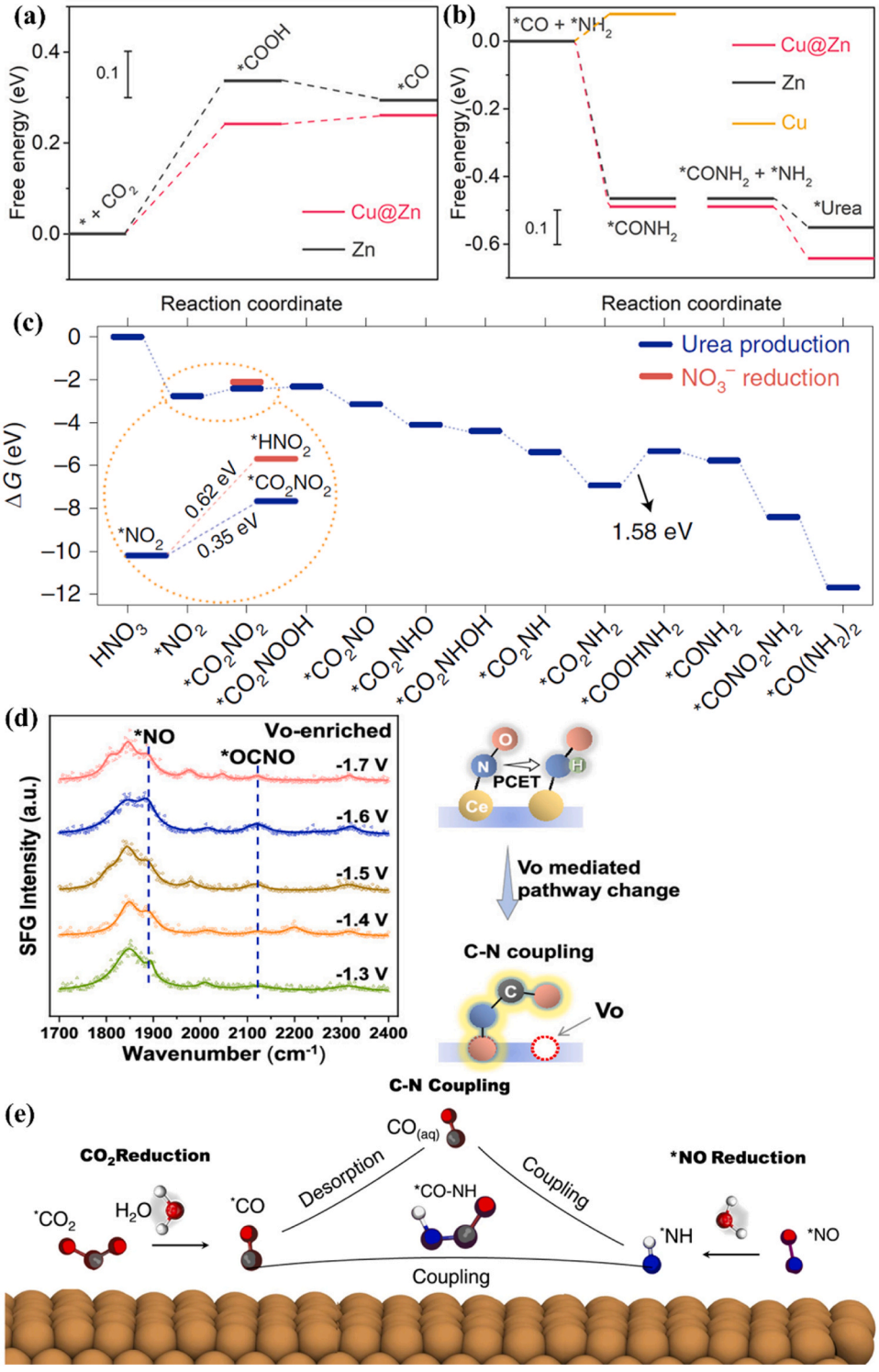

Fig. 5. Catalytic mechanism of electrocatalytic CO_2 and NO_3^- co-reduction to urea: (a) CO_2 reduction to CO and (b) C−N coupling on Cu@Zn, pure Zn, and pure Cu surfaces [25]. Copyright 2022, American Chemical Society. (c) Free-energy diagram for urea production on the {100} facets of $In(OH)_3$ at 0 V vs RHE [77]. Copyright 2021, Springer Nature. (d) SFG signals of intermediate species on Vo-CeO_2-750 (left) and schematic diagram of Vo-mediated rection pathway changes on the CeO_2 [80]. Copyright 2022, American Chemical Society. (f) schematic diagrams for two different routes of C−N coupling surface-mediated coupling of *NH with *CO direct coupling with $CO_{(aq)}$ [81]. Copyright 2022, Springer Nature.

intermediates to form the C−N bond under CO_2 and NO_3^- [77]. Theoretical calculations revealed that the urea production initiated from thermodynamically spontaneous NO_3^- reductions to $*NO_2$ intermediate on the (100) facet of $In(OH)_3$. In contrast to the endothermic protonation process of the adsorbed CO_2, the successive activation and adsorption of CO_2 were impeded, thus, making it possible to improve the selectivity for the C−N coupling to form $*CO_2NO_2$ (Fig. 5c). Moreover, the authors also conducted the control experiment to prove the C−N formation at a very early stage by direct coupling of $*NO_2$ and $*CO_2$. No urea was detected when adding NH_4^+ under electrolysis in the electrolyte, further affirming the $*CO_2$ and $*NO_2$ coupling pathways. Besides, the SR-FTIR acquires the surface chemistry underpinning the fundamental thermodynamics on the catalytic interface [78], which proves that the rate-determining step is the protonation of $*CO_2NH_2$ into $*COOHNH_2$. This work systematically presented a kind of the descriptor of $*CO_2NO_2$ for urea electrosynthesis from CO_2 and NO_3^-. Subsequently, based on the C−N coupling to form $*CO_2NO_2$ pathway, Yu and Yan et al. further reported that the introduction of oxygen vacancy to reconfigure the electronic structure at the indium surface active sites could make the intermediate of $*CO_2NO_2$ firstly transfer to $*CO_2NH_2$ via PCET and further lower the energy barrier for the conversion of $*CO_2NH_2$ into $*COOHNH_2$ from theoretical simulation results [78]. Recently, Qin and co-worker also reported that the electron-rich MoO_x nanocluster with highly unsaturated metal sites improve the rate-determining step that is the protonation of $*CO_2NO_2$ into the $*CO_2NOOH$ intermediates for urea electrosynthesis via the co-reduction of CO_2 and NO_3^- [79]. Even though, other nitrogen intermediates such as $*NH_x$ are likely to be more nucleophilic and thus more reactive than $*NO_2$. Moreover, there is not directly evidence to confirm the intermediates formation of $*CONO_2$ and the rate-determining step of $*CO_2NH_2$ conversion $*COOHNH_2$.

Very recently, a kind of new the C−N coupling pathway was proposed by Wang et al. [80]. The intermediate species of *NO inserted into oxygen vacancy conductive to couple with *CO intermediate rather than the occurrence of protonation was revealed by SFG (Fig. 5d). The control experiment suggested that urea was indeed derived from the co-reduction reaction of CO_2 and NO_3^-. And the oxygen vacancy-mediated pathway change was validated by in situ SFG spectroscopy with the appearance of *OCNO intermediate species as the descriptor [80]. DFT calculations investigated the urea electrosynthesis reaction mechanism, demonstrating that the formed *OCNO intermediate via C−N coupling was hydrogenated by the PCET process. Currently, this study is only direct to confirm the key intermediate formation of *OCNO. More importantly, the construction oxygen vacancy over catalyst can largely improve the formation of intermediate*OCNO and further enhance selective to produce urea as well as facilitate the mechanism analysis of urea formation at the catalytic interface.

Latterly, Wang and Jiang et al. also reported that the urea formation over diatomic Fe−Ni catalyst is through the coupling of *NH and *CO to form the first C−N bond and subsequent the second C−N bond, and both are thermodynamic spontaneous and highly kinetic feasible with low energy barriers on the bonded Fe−Ni pair site, respectively [24]. Moreover, the formation of the intermediate*CONH was directly revealed by SR-FTIR. More interestingly, Jiao and Qiao et al. also discovered that the *NH and *CO on Cu (100) surface in neutral electrolytes are the key precursors for C−N bonds formations at low overpotential, while at high overpotential the C−N coupling occurs between the absorbed *NH and the solvated CO (Fig. 5e) [81]. This study is firstly time to uncover the pH effect of electrolyte for the C−N coupling pathway. In a word, the two studies showed a new sight for two times C−N coupling process from CO_2 and NO_3^- to form urea, and the first time C−N coupling to form *CONH is still the key to form urea.

Owing to the low activation energy of NO_3^-, NO_2^- and NO, the pathway of photocatalytic CO_2 coupling with $NO_3^-/NO_2^-/NO$ was reported at past thirty years [82,83]. However, the developed photocatalysts are mainly concentrated on TiO_2-based materials, which is attributed to the appropriate band structure of TiO_2, unfortunately, the light absorption of TiO_2 mainly response to ultraviolet region. Even though, these studies did some meaningful exploration [82–84], particularly, the pathway of photocatalytic C−N coupling to produce urea.

At the early stage, the pathway of photocatalytic CO_2 coupling with NO_3^- to produce urea was firstly reported by Yoneyama and Liu et al. in 1998 using TiO_2 nanocrystals embedded in SiO_2 matrices as photocatalyst [83]. This study indicated that the selectivity of urea and NH_3 production can be improved by increasing the dielectric constants of solvents, but the parallel product selectivity of CO and HCOOH decreases, and the reduction reaction of NO_3^- is conductive to the urea formation. Therefore, it can be concluded that the CO and HCOOH may be the key intermediate for urea formation and improving the concentration of NO_3^- in dispersed solution can facilitate the urea formation, therefore the C−N coupling pathway should be CO or HCOOH binding with N-containing intermediate from the reduction reaction of NO_3^-. Subsequently, the combinations of carbon and nitrogen compounds were used to explore the photocatalytic C−N coupling to produce urea pathways, reported by Yoneyama and Kuwabata et al.[82], including CO_2 $-NO_3^-$, $CO-NO_3^-$, $HCOOH-NO_3^-$, CO_2 $-NH_2OH$, and CO_2 $-NO$. Interestingly, the result of the control experiments suggested that the higher selectivity of urea production is via the pathway of the photocatalytic CO_2 coupling with NO rather than NH_2OH and NO_3^-, and the higher selectivity of urea production is through the pathway of the photocatalytic NO_3^- coupling with HCOOH rather than CO_2 and CO [82]. Therefore, based on the mentioned studies, the most possible key pathway of the photocatalytic C−N coupling to form urea from CO_2 and NO_3^- should be *COOH binding with *NO. But there is still the other possibility due to the feasibility of the NH_2OH coupling with CO_2 to produce urea, such as $*NH_3/NH_{3(aq)}$ binding with *COOH. Kumari et al. further confirmed that this kind possibility of the C−N coupling to form urea via in situ generated NH_3 and CO_2 to synthesize urea [17]. The speculative C−N coupling mechanism is through the intermediate formation of HN=C=O and subsequently combined with PCET process to form $HCONH_2$. Therefore, there are several possible pathways for the photocatalytic C−N coupling to form urea from CO_2 and $NO_3^-/NO_2^-/NO$. In all, these studies could not clearly reveal the surface catalytic reaction mechanisms of urea photosynthesis.

3. The development of photo/electrocatalysts for urea synthesis

Taking account for the above challenges for urea synthesis, the development of electrocatalysts has recently attracted much attention [37,46]. The performance of urea synthesis via both the CO_2 coupling with N_2 and the CO_2 coupling with $NO_3^-/NO_2^-/NO$ is still not so desirable owing to the electronic density distribution difference between CO_2 and N_2 reactants and the large activation difference between CO_2 and $NO_3^-/NO_2^-/NO$. Currently, the development of the electrocatalysts generally demonstrates that the dual-site tandem structure is favorable for the adsorption and coactivation of carbon and nitrogen reactants, particularly, alloy nanoparticles [29,46,85,86], metal-organic frameworks with host-guest molecular structure [26,54], Mott-Schottky heterostructure [66,77], defective engineering to establish electron-deficient and electro-rich sites [27,53,78,80], single atoms and clusters catalyst [69,76,87], dual-atomic catalyst [24,45,88], and metal-free electrocatalyst [89,90]. Herein, we will provide a comprehensive overview of electrocatalysts that have achieved catalytic performance for urea synthesis.

For urea photosynthesis from CO_2 and $N_2/NO_3^-/NO_2^-/NO$, TiO_2-based photocatalysts have already exhibited a huge potential [16]. For instance, for photocatalytic co-reduction of CO_2 and NO_3^- to produce urea, the quantum size effect of TiO_2 nanocrystal was revealed that TiO_2 nanocrystal showed a greater performance for the photocatalytic urea synthesis compared with bulk TiO_2 particles (P25) [82]. Moreover, in contrast to TiO_2 nanocrystal colloidal, the TiO_2 nanocrystal immobilized on polypyrrolidinone (PVPD) film displayed a remarkable performance

for urea formation in propylene carbonate solution, rather than aqueous solution [82]. Cu SA-TiO_2 and Ti^{3+}−TiO_2 all showed a decent performance for urea synthesis from CO_2 and N_2 [48,71], Besides, the dispersed micro-environment of TiO_2-based photocatalysts was adjusted and the substrate of TiO_2-based photocatalysts was also modified for urea synthesis [16,83]. However, compared to urea electrosynthesis, the development of urea photosynthesis stays still at early stage. Therefore, it is a promising avenue to develop appropriate photocatalysts, photocatalytic system configurations such as suspension system and catalyst particle loaded on substrate system, and more in situ techniques combined with theoretical simulations to detect urea formation mechanism.

3.1. Electrocatalysts for urea synthesis from N_2 and CO_2

Urea electrosynthesis from CO_2 and N_2 co-reduction was firstly investigated by Kayan et al. under high-pressure condition (30 bar N_2 + 30 bar CO_2), a polypyrene or polyaniline-coated platinum electrode displayed the optimum 0.085 mA cm^{-2} of urea production rate and 6.9% of Faradaic efficiency (FE) achieved at − 0.325 V vs NHE [61]. Although this study is pioneering, it is still hard to demonstrate how this electrode is conductive to urea synthesis from CO_2 and N_2 due to the high-pressure condition. Remarkably, Chen and Wang et al. constructed PdCu nano-alloy on the surface of oxygen vacancy rich TiO_2 nanosheets (PdCu-TiO_2) via the chemical co-reduction strategy, and the urea of yield rate is reach to 3.36 mmolg^{-1} h^{-1} at − 0.4 V vs RHE with an optimized flow cell, and the corresponding FE was 8.92% under ambient condition (Table 1 and Fig. 6a) [46]. In this study, PdCu nanoparticles were considered as active sites for urea electrosynthesis from CO_2 and N_2, the C of CO_2 is adsorbed on the side of Cu in nano-alloy, N_2 is adsorbed on the side of Pd in nano-alloy via side-on configuration. Unfortunately, the adsorption configuration of N_2 on electrocatalyst was also reported via end-on configuration [91–93]. Perhaps, the C−N coupling pathway is through *CO binding with the end-on configuration of N_2 rather than side-on configuration. Moreover, the oxygen vacancy on TiO_2 nanosheets produce Ti^{3+} sites [75], which can also be regarded as active sites for urea synthesis. Thus, there is one kind possibility of the synergy effect between PdCu nanoparticles and oxygen vacancies for urea from CO_2, N_2, and H_2O. Interestingly, Wang et al. designed two types of catalysts via vacancy-anchorage strategy: single-atom Pd_1-TiO_2 and dual-atom Pd_1Cu_1-TiO_2 nanosheets, and the dual-atom Pd_1Cu_1-TiO_2 showed a higher yield rate than single-atom Pd_1-TiO_2 for urea electrosynthesis from CO_2 and N_2 [88]. Wang and co-workers demonstrated that the synergistic effect of the Pd_1Cu_1 dual-atom and oxygen vacancy active centers plays a key role in promoting the coupling of CO_2 and N_2 over above two active sites and stabilizing the formed *NCON* intermediate over Pd_1Cu_1 sites, leading to the direct C−N coupling over Pd_1Cu_1 −TiO_2 (Fig. 6b). However, the N_2 adsorbed on the Pd atom and oxygen vacancy via the adsorption configuration of side-on, which is differ from the PdCu nanoparticles of the N_2 adsorption. The defective Cu-Bi alloy catalyst (Fig. 6c), further developed by Song et al., could currently offer a maximum urea concentration of 0.45 mg L^{-1} and the largest FE of 8.7% at − 0.4 V vs RHE due to the synergies effect for the defects and Cu-Bi alloy improving the formation of *NCON* [29]. Lai et al. designed V_N-Cu_3N-300 catalysts with tip and vacancy structures, showed a urea yield of 81 μg h^{-1} cm^{-2} and the corresponding Faraday efficiency of 28.7% (Fig. 6d) [94]. Moreover, the authors demonstrated that the tip effect promoted the adsorption and activation of CO_2 and surface nitrogen vacancies promotes the formation of *N = N * intermediates, ensuring C–N coupling, and also optimizing the dissociation process of water, providing a proton supply for the synthesis of urea. Besides, the rice-like InOOH nanoparticles with oxygen vacancy, constructed the FLPs, and exhibited a urea yield rate of 6.85 mmol h^{-1} g^{-1} and FE of 20.97% at− 0.4 V vs RHE via the adsorption configuration of the side-on for N_2 [95]. Therefore, the vacancies or defects over catalysts as active center is favorable for the adsorption and activation of N_2 via side-on. Zhang et al. also constructed several kinds of dual sites tandem electrocatalysts, for example, in the case of Mott-Schottky Bi-$BiVO_4$ heterostructures via in situ chemical reduction strategy (Fig. 6e), this catalyst realized a high urea yield rate of 5.91 mmol h^{-1} $g^{-1}$and a FE of 12.55% at − 0.4 V vs RHE. N_2 is adsorbed on the $BiVO_4$ side via side-on way and the C of CO_2 is adsorbed on the Bi side in Mott-Schottky heterostructures [66]. Similarly, a $BiFeO_3$/$BiVO_4$ heterojunction was also prepared via epitaxial growth method, and a urea yield rate of 4.94 mmol $h^{-1}g^{-1}$ with a FE of 17.18% at − 0.4 V vs RHE was achieved [53]. Besides, a host-guest molecular of MOF Co-PMDA-2-mblM (Fig. 6f) and $Ni_3(BO_3)_2$-150 (Fig. 6g) as artificial frustrated Lewis pairs (FLP) was synthesized via self-assembly approach, and they attained a current high urea yield rate of 14.47 mmol $h^{-1}g^{-1}$ and FE of 48.97% at − 0.5 V vs RHE, and a urea yield rate of 9.70 mmol $h^{-1}g^{-1}_{cat}$ and FE of 20.36% at − 0.5 V vs RHE, respectively [26,54]. Zhang et al. considered that the involved host-guest interaction not only generated the desirable local electrophilic and nucleophilic regions, but also achieved the evolution from the high spin state of Co^{3+} (HS $t_{2g}^4e_g^2$) to the intermediate spin state of Co^{4+} (IS $t_{2g}^4e_g^1$) in CoO_6 octahedron, realized the targeted chemisorption and activation of the N_2 and CO_2 molecules via bonding orbital and antibonding orbital [54]. Moreover, Zhang et al. revealed that the electron-deficient LA in sites and electron-rich LB In-OH achieved the targeted chemisorption of the N_2 and CO_2 molecules by electronic interaction respectively [96]. Based on the above Zhang et al.'s works, we can conclude that this kind of the σ orbital carbonylation strategy, proposed by Zhang and collaborators, enable achieve the target adsorption of N_2 and CO_2 molecules on the constructed local electrophilic and nucleophilic regions respectively, adequately demonstrated that the dual-site concept is a reasonable and effective direction for the design of urea electrosynthesis. Interestingly, Copper phthalocyanine nanotubes as electrocatalyst, developed by Chorai et al., exhibited a urea yield of 143.47 μg h^{-1} mg^{-1}_{cat} and faradaic efficiency of 12.99% at −0.6 V vs RHE, and theoretical

Table 1
The reported electrocatalysts for urea synthesis from CO_2 and N_2.

Electrocatalyst	Urea formation rate (Applied potential)	FE (Reaction device)	Electrolyte condition (Gas flow rate)
PdCu/TiO_2[46]	0.12 mmol $g^{-1}h^{-1}$(−0.4 V) 3.36 mmol $g^{-1}h^{-1}$(−0.4 V)	0.66% (Flow cell) 8.92% (Flow cell)	0.1 M $KHCO_3$ 30 sccm (1:1 v/v)
Bi-$BiVO_4$ hybrid [66]	5.91 mmol $g^{-1}h^{-1}$(−0.4 V) 6.64 mmol $g^{-1}h^{-1}$(−0.4 V)	12.55% (H-cell) 12.55% (H-cell)	0.1 M $KHCO_3$ 30 sccm (1:1 v/v)
Co-PMDA-2-male [54]	14.47 mmol $g^{-1}h^{-1}$(−0.5 V)	48.97%(H-cell)	0.1 M $KHCO_3$
$BiFeO_3$/$BiVO_4$ hybrids[53]	4.94 mmol $g^{-1}h^{-1}$ (−0.4 V) 5.42 mmol $g^{-1}h^{-1}$ (−0.4 V)	17.18%(H-cell) 20.75%(H-cell)	0.1 M $KHCO_3$ (Bmim)BF_4-$KHCO_3$
InOOH nanoparticles [95]	6.85 mmol $g^{-1}h^{-1}$ (−0.4 V)	20.97%(H-cell)	0.1 M $KHCO_3$
$Ni_3(BO_3)_2$ − 150 [26]	9.70 mmol $g^{-1}h^{-1}$ (−0.5 V)	20.36%(H-cell)	0.1 M $KHCO_3$
Defective Cu-Bi alloy[29]	5.27 mol s^{-1} cm^2 (−0.4 V)	8.7% (H-cell)	0.1 M $KHCO_3$
Copper Phthalocyanine Nanotubes[69]	2.19 mmol $g^{-1}h^{-1}$ (−0.6 V)	10.04% (H-cell)	0.1 M $KHCO_3$
Pd_1Cu_1-TiO_2[88]	166.67 mol_{urea} $mol_{pd}^{-1}h^{-1}$ (−0.6 V)	22.54% (H-cell)	0.1 M $KHCO_3$
VN-Cu_3N-300[94]	81 μg h^{-1} cm^{-2}	28.7% (H-cell)	0.1 M $KHCO_3$
MoP[97]	12.4 μg h^{-1} mg^{-1}	36.5% (H-cell)	0.1 M $KHCO_3$
Zn-Mn diatomic catalyst[70]	4.14 mmol $g^{-1}h^{-1}$ (−0.3 V)	63.5% (H-cell)	0.1 M $KHCO_3$

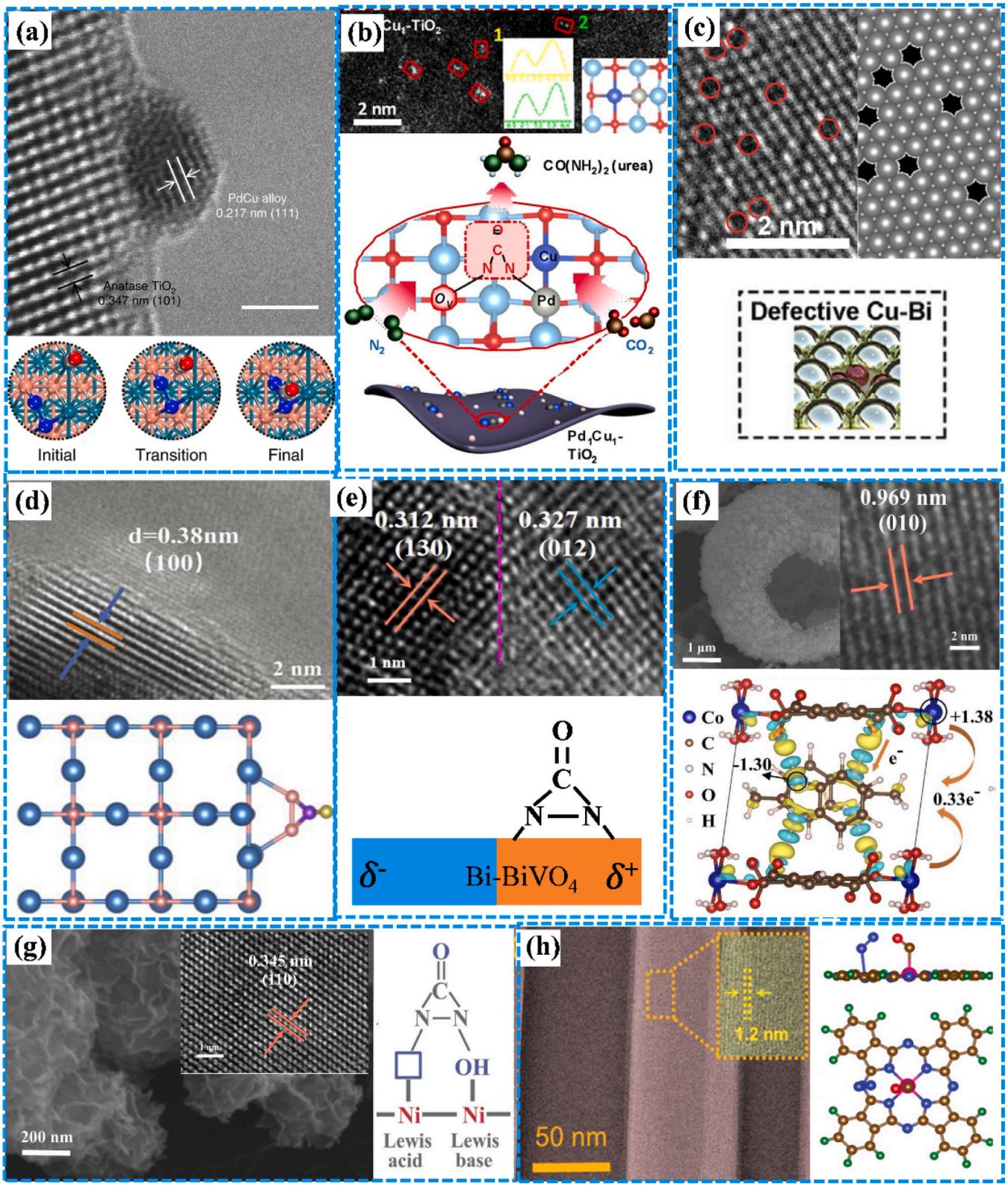

Fig. 6. Electrocatalysts for CO_2 and N_2 co-reduction to urea. (a) High-resolution transmission electron microscopy (HRTEM) image of PdCu/TiO_2 and the formation process of *NCON* [46], Copyright 2020 Springer Nature. (b) HRTEM image of Pd_1Cu_1/TiO_2 with oxygen vacancies and the *NCON*formation over Pd_1Cu_1/TiO_2 [88], Copyright 2021, Wiley & Sons, Inc. (c) HRTEM and model image of defective Cu-Bi alloy [29]. Copyright 2022, Elsevier Inc. (d) HRTEM image of V_N-Cu_3N-300 and the formation of *NCON* [94], Copyright 2023, Wiley & Sons, Inc. (e) HRTEM image of Bi-$BiVO_4$ and the *NCON*formation illustration [66], Copyright 2021, Wiley & Sons, Inc. (f) SEM and HRTEM image and charge density difference of Co-PMDA-2-male [54], Copyright 2022, Royal Society of Chemistry. (g) SEM and HRTEM image of $Ni_3(BO_3)_2$-150 and the *NCON*formation over $Ni_3(BO_3)_2$-150 [26], Copyright 2021, Royal Society of Chemistry. and (h) HRTEM image of CuPc nanotube and the adsorption configuration of N_2 and CO_2 [69]. Copyright 2022, Wiley & Sons, Inc.

calculation suggests that pyridinic-N_1 and Cu centers are responsible to form C−N bonds for urea by co-reduction of N_2 to N = N * and CO_2 to *CO, respectively (Fig. 6h) [69]. This work differs from the previous works due to the adsorption site of N_2 on pyridinic-N_1 via end-on configuration, rather than via side-on. Therefore, this work provides the new mechanistic insight about urea electrosynthesis from N_2 and CO_2 in a single molecule catalyst and rational design of efficient noble metal-free electrocatalysts. Besides, inspired by the dual-site concept, Wang et al. further reported that a Zn-Mn diatomic catalyst exhibited the current highest Faradaic efficiency of 63.5% and a high urea yield rate of 4.14 mmol $g^{-1}h^{-1}$ at the potential of − 0.3 V vs RHE (Table 1) [70]. It is worthy to note that the Cl-coordinated Zn-Mn sites are far superior to the atomic ZnMn-N sites, the several diatomic metal sites with or without Cl-coordinated, and the atomic Zn or Mn metal sites. This study gains a huge breakthrough that the C−N coupling to form urea reaction dominates for the CO_2 and N_2 electro-reduction, rather than the side reactions such as NRR, CO_2RR, and HER. Therefore, designing and constructing dual-site structure is beneficial for the co-adsorption, activation and coupling process of multiple reactants, particularly, CO_2 and N_2 as reactants with highly chemical inert. Furthermore, the above electrocatalysts for the performance of urea have been summarized in Table 1.

3.2. Photocatalytic urea synthesis via the co-reduction of N_2 and CO_2

Currently, Ti^{3+}-doped TiO_2 loaded on Fe-CNTs (Ti^{3+}-TiO_2/Fe-CNTs) is prepared through the vapor deposition method and thermal reduction, and showed a 177.525 μmol g^{-1} h^{-1} of the urea yield rate as the N_2/CO_2 with 100 mL min^{-1} flow rate [71]. In this study, the one-dimensional Fe-CNTs as substrates are obtained via the vapor deposition method with coal as s carbon source. Ti^{3+}-TiO_2 was loaded on the Fe-CNTs, improved the charge carrier separation and migration, thereby attained a greater photocurrent density than pure Ti^{3+}-TiO_2. Ti^{3+} doping concentration in TiO_2 can be adjusted through the reduction method of $NaBH_4$, which enable to tune the band structure and light adsorption of photocatalyst. Besides, Ti^{3+} doping concentration in TiO_2 is positively correlated with the NH_3 yield and the arrangement of Ti^{3+} and the adjacent oxygen vacancy is closely related to urea formation, agreed to that the vacancy over electrocatalyst is favorable for urea synthesis from co-reduction of CO_2 and N_2. Besides, Zhang et al. reported Cu SA-TiO_2 showed a considerable rates of urea production, attributed that the expedited dynamics behaviors originating from reversible single-atom copper over Cu SA-TiO_2 allow the assurance of abundant and continual photogenerated electrons for multi-electron-demanding co-photoactivation of N_2 and CO_2 [48]. Currently, Li et al. developed a solar urea synthesis route from N_2, CO_2 and H_2O with S defected $ZnIn_2S_4$ ($ZnIn_2S_{4-x}$, ZIS) flowerlike microspheres as photocatalyst and NiCoP nanoparticles as co-catalyst. Among of 15%-NCP/ZIS showed a urea conversion rate of 13.9 μmol g^{-1} h^{-1} at ambient temperature and 1 bar, and further increased to 19.6 μmol g^{-1} h^{-1} with mild rising temperature (80 ℃) and pressure (10 bar) [72].

3.3. Electrocatalysts for urea synthesis from CO_2 and $NO_3^-/NO_2^-/NO$

Although N_2 is economically the best N precursor because of its accessibility from air and direct urea electrosynthesis using N_2 could lower the material cost and circumvent the energy-intensive fossil-fuel-based Haber-Bosch process, the kinetic N_2 electroreduction is exceedingly sluggish due to the extreme stability of the N≡N bond [38], which limits the overall rate of urea generation. Reported partial current densities for urea formation is usually below 10 or even 1 mA cm^{-2}, much lower than the rates achieved from CO_2 coupling with NO_3^-/NO_2^- co-reduction [44,98]. In contrast to N_2 as nitrogen source for urea electrosynthesis, although NO_3^-/NO_2^- is kinetically more favorable. The effluents with a high concentration of NO_3^-/NO_2^- as nitrogen source, the electrochemical reduction of NO_3^-/NO_2^-coupling with CO_2 into recyclable urea seems more alluring [99]. Besides, the discharged NO contaminants could be recycled as feedstock for urea electrosynthesis and the NO of the containing N = O bond is a crucial intermediate for NO_3^-/NO_2^- reduction [33]. Therefore, it has a huge potential for using NO as a nitrogen source to couple with CO_2 to produce urea.

The urea electrosynthesis from CO_2 and $NO_3^-/NO_2^-$was first uncovered by Shibata and Furuya et al. by using a Cu-loaded gas diffusion electrode in 1995 [18]. Urea production was confirmed in both CO_2 + NO_3^- and CO_2 + NO_2^- co-reductions at − 0.75 V, corresponding to an FE of 10% and 37%, respectively. Subsequently, various metals, metal boride, and metalphthalocyanineyanine (MPc) were loaded on gas diffusion electrodes toward the electrosynthesis of urea from CO_2 and NO_3^- or NO_2^-. The authors revealed that it was generally more difficult to form urea from NO_3^- than NO_2^- coupling with CO_2 electroreduction because of no activity of NO_3^- reduction over Au and all MPc catalysts [100]. It was also found that there is a positive linear correlation between urea of FE and $(FE(CO)*FE(NH_4^+))^{0.5}$ for these metal materials using CO_2 and NO_2^- as reactants. Although these studies are pioneeringly, there are still several critical challenges for urea electrosynthesis from CO_2 and NO_3^-/NO_2^-, particularly, the electrocatalyst development of high performance for urea synthesis.

In recent years, focusing on the challenges for the activation of reactants and the competition between multiple PCET processes and the C−N coupling step, the element doping and defects engineering strategies is firstly used to construct electrocatalyst with both electrophilic and nucleophilic sites. Saravanakumar et al. constructed by drop-casting the mixture of P25 titania and Nafion solution on an indium-doped tin oxide (ITO) electrode, and this study showed 40% of FE for urea production [101]. Then, $FeTiO_3$ nanoparticles were further developed, and also exhibited a certain performance for urea electrosynthesis from CO_2 and NO_2^- co-reduction using an undivided cell [102]. A low-valence Cu-doped TiO_2 catalyst were also explored by Zheng et al., and also obtained 43.1% of FE for urea at − 0.4 V vs RHE (Table 2) [75]. The incorporation of Cu dopants in anatase TiO_2 facilitates to form abundant oxygen vacancies and Ti^{3+} defect sites, which allows for the efficient adsorption and activation of NO_2^- and the C−N coupling. The Te-doped into Pd nanocrystals (Te-Pd NCs) achieved nearly 12.2% of FE at − 1.1 V vs RHE for urea electrosynthesis from CO_2 and NO_2^- [74]. The copper single atoms decorated on a CeO_2 support (Cu_1-CeO_2) was fabricated via wet impregnation and calcination, and showed an average urea yield rate of 52.84 mmol $h^{-1}g_{cat.}^{-1}$, which is the highest value that has ever been reported for coupling of CO_2 and NO_3^- (Table 2). The clusters of Cu_4 over Cu_1-CeO_2 is favorable for the C−N coupling step and urea formation due to the reconstitution of single Cu_1 to clusters Cu_4 during electrolysis (Fig. 7a) [87]. Unfortunately, it was neglected that the oxygen vacancies would be active centers for urea synthesis.

The oxygen vacancy-rich ZnO porous nanosheets (ZnO-V) also discovered by Zhang et al. achieved 23.26% of FE at − 0.79 V vs RHE for urea synthesis from CO_2 and NO_2^- [103]. Wang et al. also reported that tuning oxygen vacancy (Vo) concentration in CeO_2 is conductive to urea production. Vo−CeO_2 exhibited a high yield rate with 943.6 mg h^{-1} g^{-1} at − 1.6 V vs RHE (Fig. 7b) [80]. Although the element doping and vacancy engineering can construct the dual-site with the desirable local electrophilic and nucleophilic regions to improve the activation, adsorption the C−N coupling process of multi-reactants, the huge difference of activation energy of CO_2 and NO_3^-/NO_2^- is differ to the urea formation via CO_2 and N_2 co-reduction. Recently, Chen et al. reported that porous N-doped carbon electrocatalysts with various proportions of N species were controllably synthesized via pyrolysis of the coordination polymer (Fig. 7c), and the authors demonstrated that the pyridinic-N- and pyrrolic-N-induced active sites promote the NO_3RR activity but the graphitic-induced active sites tend to promote the CO_2RR activity, particularly, the most of urea yield rate reach up to 610.6 mg h^{-1} $g_{cat.}^{-1}$ due to balance the CO_2RR and NO_3RR activities (Fig. 7c) [89]. Besides, carbon nanotubes with fluorine-rich surface (F-rich CNTs) as metal-free electrocatalysts for urea synthesis from CO_2 and NO_3^-, developed by Hu et al. [73], exhibited a yield rate of 6.36 mmol h^{-1} g_{cat}^{-1} with a

Table 2
The reported electrocatalysts for urea synthesis from CO_2 and NO_3^-/NO_2^-/NO.

Electrocatalyst	Urea formation rate (Applied potential)	Corresponding FE (Reaction device)	Electrolyte condition (CO_2 flow rate)
$In(OH)_3$[77]	533.1 ug $h^{-1}mg_{cat.}^{-1}$ (−0.6 V vs RHE)	53.5% (H−cell)	0.1 M KNO_3 (20 sccm)
O_v-In(OOH) [78]	592.5 ug $h^{-1}mg_{cat.}^{-1}$ (−0.5 V vs RHE)	51.0% (H−cell)	0.1 M KNO_3 (20 sccm)
Cu@Zn Nanowires [25]	7.29 μmol $cm^{-2}h^{-1}$ (−1.02 V vs RHE)	9.28% (H−cell)	0.2 M $KHCO_3$ + 0.1 M NO_3^-(20 mL min^{-1})
Cu SACs (Cu-Nx)[76]	4.3 nmol s^{-1} cm^{-2} (−0.9 V vs RHE)	28% (H−cell)	0.1 M $KHCO_3$ and 0.1 M KNO_3 (N/A)
Vo-CeO_2-750 [80]	943.6 mg $h^{-1}g^{-1}$ (−1.6 V vs RHE)	3.9% (H-cell)	0.1 M $KHCO_3$ + 50 mM KNO_3 (30 mL min^{-1})
B-FeNi DSAC [24]	20.2 mmol $h^{-1}g^{-1}$ (−1.5 V vs RHE)	17.8% (H-cell)	0.1 M $KHCO_3$ + 50 mM NO_3^-/NO_2^- (30 mL min^{-1})
TiO_2-Nafion [101]	N/A	40.0%(H−cell)	CO_2-saturated 0.1 M KNO_3
Co-NiOx@GDY [28]	913.2 μg h^{-1} mg_{cat}^{-1} (−0.7 V vs RHE)	64.3% (H-cell)	CO_2-saturated 0.01 M $NaNO_2$
ZnO-V[103]	16.56 umol $h^{-1}cm^{-2}$ (−0.79 V vs RHE)	23.26% (H−cell)	0.2 M $NaHCO_3$ + 0.1 M $NaNO_2$
Te-doped Pd NCs[74]	0.475 wt% h^{-1} in 10 mL (−1.1 V vs RHE)	12.2% (Flow cell)	0.1 M $KHCO_3$ + 0.05 M KNO_2 (30 sccm)
Cu-doped TiO_2 [75]	20.8 umol h^{-1} (−0.4 V vs RHE)	43.1% (H-cell)	0.2 M $KHCO_3$ + 0.02 M KNO_2
AuCu nanofibers [104]	3889.6 μg h^{-1} $mg_{cat.}^{-1}$ (−1.55 V vs Ag/AgCl)	24.7% (H-cell)	0.5 M $KHCO_3$ + 0.01 M KNO_2
Zn nanobelts [27]	15.13 mmol $h^{-1}g^{-1}$	11.26% (Flow cell)	0.2 M $KHCO_3$ (molar ratio NO: CO_2 =3:7)
F-rich CNT [73]	6.36 mmol $h^{-1}g^{-1}$ (−0.65 V vs RHE)	18.0% (Flow cell)	0.1 M KNO_3 (30 mL min^{-1})
Fe(a)@C-Fe_3O_4/CNTs [105]	1342.3 μg h^{-1} $mg_{cat.}^{-1}$ (−0.65 V vs RHE)	16.5% (H-cell)	CO_2-saturated 0.1 M KNO_3 (30 mL min^{-1})
Cu with atomic spacings [106]	7541.9 μg h^{-1} $mg_{cat.}^{-1}$ (−0.41 V vs RHE)	51% (Flow cell) (115.25 mA cm^{-2})	CO_2-saturated 0.1 M KNO_3 (30 mL min^{-1})
CuIn-C[85]	13.1 mmol $h^{-1}g^{-1}$ (−1.4 V vs RHE)	/ (H-cell)	CO_2-saturated 0.1 M KNO_3 (30 mL min^{-1})
N-doped Carbon[89]	610.6 mg h^{-1} $mg_{cat.}^{-1}$ (−1.5 V vs RHE)	/ (H-cell)	CO_2-saturated 20 mM KNO_2 (30 mL min^{-1})
MoO_x/C[79]	1431.5 μg h^{-1} $mg_{cat.}^{-1}$ (−0.6 V vs RHE)	27.7% (H-cell)	CO_2-saturated 0.1 M KNO_3 (30 sccm)
Cu_1–CeO_2[87]	52.84 mmol h^{-1} $mg_{cat.}^{-1}$ (−1.6 V vs RHE)	/ (H-cell)	CO_2-saturated 50 mM KNO_3 (30 mL min^{-1})

corresponding FE of 18% at − 0.65 V vs RHE. Therefore, balancing the activation efficiency of CO_2 and NO_3^-/NO_2^- and it's involved parallel reaction should be deemed as a crucial principle for the development of catalysts.

The bimetallic catalysts are also regarded as the candidates for urea synthesis due to the electronic structure of carbon and nitrogen reactants. Self-supported core-shell Cu@Zn nanowire was constructed through an electroreduction method, which exhibited the superior performance of urea electrosynthesis from CO_2 and NO_3^- with 7.29 μmol cm^{-2} h^{-1} of yield rate and 9.28% of FE at − 1.02 V vs RHE (Fig. 7d) [25]. Ultra-thin AuCu alloy nanowires, developed by Wang et al., provided much high energetically active interface between Au and Cu, and it achieved a yield rate of up to 3.8896 mg h^{-1} $mg_{cat.}^{-1}$ and a FE of 24.7% of − 0.9 V vs RHE for urea production from CO_2 and NO_2^- [104]. Cobalt-nickel mixed oxides supported by graphdiyne materials (Co-N-iOx@GDY) showed a yield rate of 913.2 μg h^{-1} $mg_{cat.}^{-1}$ and a high FE of 64.3% for urea synthesis [28], which may be attributed by the facile accessibility of Co-NiO_X as active sites on graphdiyne and more abundant of the heterostructure than the interface alloy and Mott-Schottky junction (Fig. 7e). Graphitic carbon encapsulated amorphous iron and iron oxide nanoparticles on carbon nanotubes (Fe(a)@C-Fe_3O_4/CNTs) exhibited a urea yield of 1341.3 ± 112.6 μg h^{-1} mg_{cat}^{-1} and a FE of 16.5 ± 6.1% [105]. An indium hydroxide $In(OH)_3$ catalyst for urea electrosynthesis from NO_3^- and CO_2 realized highly selective urea production with a ultra-high FE of 53.4% at − 0.6 V vs RHE [77], which is owing to the Mott-Schottky junction and the exposed (100) facets of $In(OH)_3$. Recently, Wang and co-workers also developed the CuIn bimetallic loaded on carbon black as electrocatalyst, and showed a urea yield rated of 13.1 mmol g^{-1} h^{-1} (Fig. 7f) [85]. And the authors proposed that the urea synthesis activity is closely linked with the localized surface charge on bimetallic electrocatalysts, it is found that a negatively charged surface induces C-bound path and boosts urea synthesis (Fig. 7f).

The effect of the different crystalline facets was revealed for urea electrosynthesis. Afterwards, an indium oxyhydroxide (InOOH) with Vo was constructed by defect-engineering, attained a high FE of 51.0% and an outstanding average urea yield of 592.5 ug h^{-1} mg_{cat}^{-1} at − 0.5 V vs RHE, which was ascribed to the preferential breakage of the In-O bond on the unsaturated In atom [78]. Kwon and co-workers reported the copper (Cu) with atomic-scale spacings (ds) between copper facets significantly improved the electrochemical synthesis of urea from co-reduction CO_2 and NO_3^- due to the lithiation approach to create ds between the copper facets (Fig. 7g) [106]. Moreover, Cu with d_s close to 6 Å achieves a remarkably high urea yield rate of 7541.9 μg h^{-1} mg_{cat}^{-1} and partial current density of 115.25 mA cm^{-2}, substantially greater than the bare Cu (urea yield rate of only 444.7 μg h^{-1} mg_{cat}^{-1}) counterpart because of atomic-scale spacing enhancing the C−N bond formation kinetically and thermodynamically (Fig. 7g).

Single atom or dual atom catalysts (SACs/DASC) were further used to urea electrosynthesis from CO_2 and NO_3^-, Cu-N-C SACs achieved a 28% of FE and a yield rate of 4.3 nmol s^{-1} cm^{-2} at −0.9 V vs RHE for urea production [76]. Cu-N_4 sites exhibited a higher intrinsic activity toward the CO_2RR, whilst both Cu-N_4 and Cu-N_{4-x}-C_x sites were active toward NO_3^-RR. Therefore, although SACs obtained a decent performance for urea synthesis, it is difficult to balance the competition between the PCET process and the C−N coupling process due to the isolated single active site. Recently, Wang and jiang et al. reported that diatomic Fe–Ni catalyst (B-FeNi-DASC) showed a high urea yield rate of 20.2 mmol h^{-1} g^{-1} with corresponding FE of 17.8%, which was far higher than single-atom (Fe or Ni) and isolated diatomic catalyst (Fig. 7h) [24]. And the total FE of CO, NH_3 and urea was closed to 100%, indicating that the bonded Fe–Ni pairs could eliminate the competition of HER. Even so, the parallel reduction reaction of reactants is not still alleviated on DASC, ascribed to the unbalance between the PCET process and the C−N coupling process on the Fe–Ni pairs (Fig. 7h).

Lastly, NO as nitrogen sources was also used to couple with CO_2 to produce urea. Ten kind of bulk metal catalysts were used to the electrocatalytic CO_2 and NO co-reduction to urea [27], among of them, Zn foil exhibited the highest urea yield rate and corresponding to a maximum value of 1.12% under −0.92 V vs RHE. Subsequently, Zn nanobelts was constructed through the in situ electrochemical reduction, showed a yield rate of 15.13 mmol h^{-1} g^{-1} and corresponding FE of 11.26% at~40 mA cm^{-2} in a flow cell. Although NO contains a weaker N = O bond than the N≡N bond of N_2, the kinetic process is sluggish due to the mass transport limitation of NO, causing the large competition reaction of HER.

In all, in comparison with all electrocatalysts (Table 2), Cu_1-CeO_2 showed currently the highest selectivity of urea synthesis in CO_2-saturated 0.1 M NO_3^- solution [87]. Even so, it needs still to identify the key

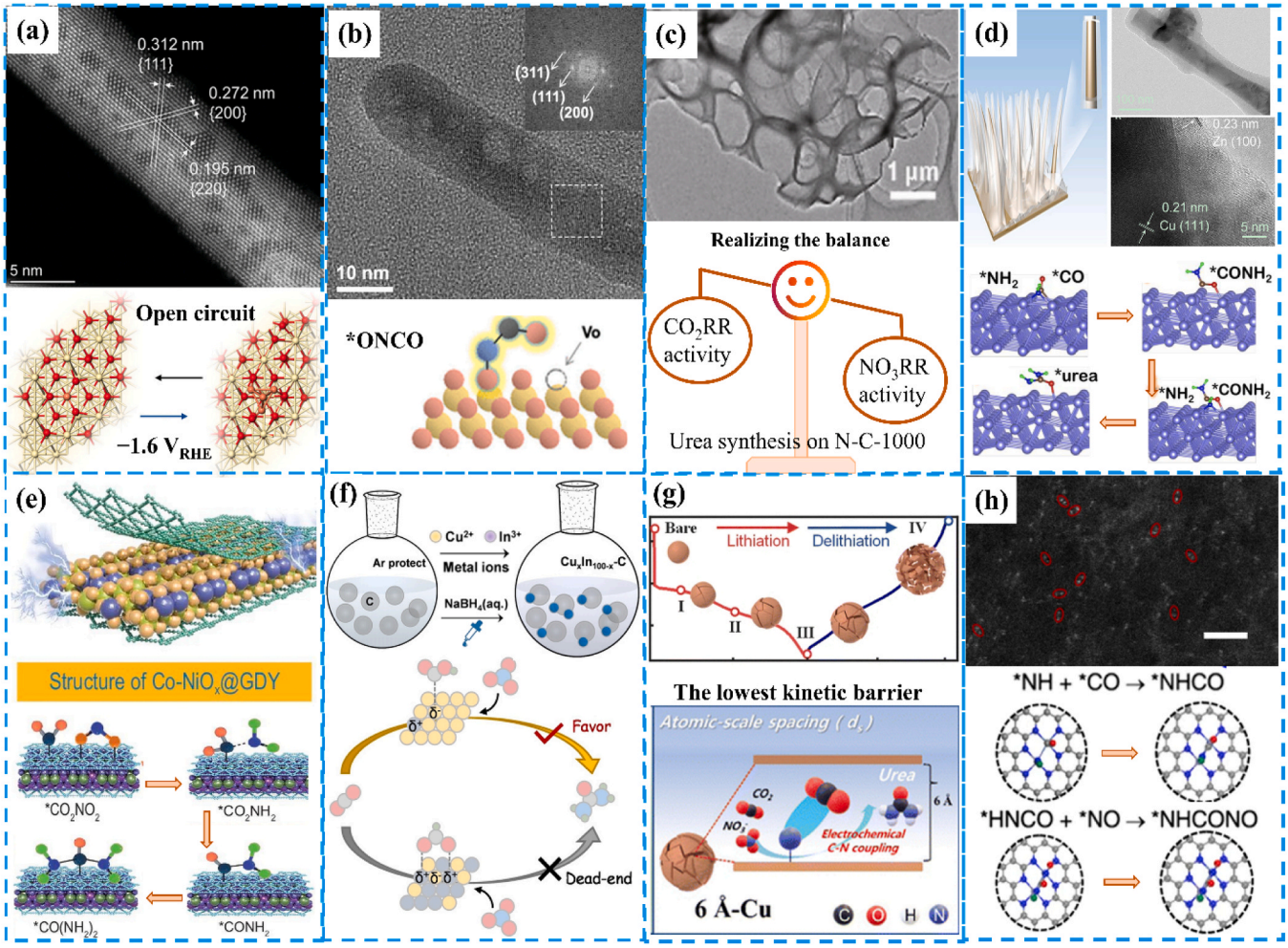

Fig. 7. Electrocatalysts for CO_2 and NO_3^-/NO_2^-/NO co-reduction to urea. (a) HRTEM image of Cu_1-CeO_2 and the dynamic reconstitution for Cu_1 to Cu_4 [87]. Copyright 2023, Wiley & Sons Inc. (b) HRTEM image of Vo-CeO_2 and the *ONCO formation via oxygen-vacancy [80]. Copyright 2022, American Chemical Society. (c) HRTEM image of N-C-1000 and balancing the sub-reaction activity [89]. Copyright 2023, Wiley & Sons Inc. (d) Illustration and TEM image of core-shell Cu@Zn nanowire and the formation process of urea over Cu@Zn [25]. Copyright 2022, American Chemical Society. (e) Schematic illustration of Co–NiOx@GDY and the formation process of urea over Co–NiOx@GDY [28]. Copyright 2022, by Oxford University Press. (f) The preparation of bimetallic CuIn-C and the localized negatively charged surface is superior to the positively charged [85]. Copyright 2023, Wiley & Sons Inc. (g) Lithiation and delithiation process of Cu_2O and schematical diagram of Cu surface with a spacing of d_s (6 Å) for urea synthesis [106]. Copyright 2023, Royal Society of Chemistry. (h) HRTEM image of B-FeNi-DASC and schematical illustration of two C−N coupling process [24]. Copyright 2022, Springer Nature.

descriptor and reveal its formation mechanism on catalyst for urea formation from CO_2 and NO_3^-/NO_2^-/NO because of the several pathways of urea synthesis. Generally, it is required to analyze the formation mechanism of the key intermediate and conclude the key factor for each component, such as the electronic structure feature of active site over catalyst, the distribution of active site over catalyst, the microstructure of catalyst, the pH and ion concentration of the electrolyte, and the selectivity of reactants. More importantly, the development of catalysts should consider how to balance the activation and adsorption of CO_2 and NO_3^-/NO_2^-/NO, the parallel reaction, the PCET process, and the C−N coupling process.

3.4. Photocatalytic urea synthesis from CO_2 and $NO_2^-/NO_3^-/NO$

Inspired by the urea electrosynthesis from CO_2 and NO_2^-/NO_3^- on a Cu-loaded gas diffusion electrode [18], subsequently, several studies reported urea photosynthesis on TiO_2-based materials as photocatalysts [82,83,107]. Liu and Yoneyama et al. firstly reported that TiO_2 nanocrystal immobilized in PVPD film (Q-TiO_2/PVPD) showed a greater performance of urea formation from CO_2 and NO_3^- than TiO_2 nanocrystal colloidal in polypropylene carbonate solution [82], which may be ascribed to the improvement of photo-generated electron-hole pairs separation at the interface between TiO_2 nanocrystal and PVPD and the light adsorption of PVPD. In this study, although TiO_2 nanocrystal loaded on PVPD film decrease the specific surface area of TiO_2 nanocrystal compared to colloidal, the surface electron density on Q-TiO_2/PVPD should be larger than colloidal. Besides, compared with bulk TiO_2 nanoparticle, TiO_2 nanocrystal showed a higher activity of urea formation, attributed to the larger specific surface area and effective photo-generated electron-hole pairs separation. The authors also concluded that using Q−TiO_2 in the suspension increased the collision frequency and interaction between urea and the catalyst surface, causing the urea photodegradation [82]. Moreover, in contrast to the dispersion of TiO_2 nanocrystal directly into an aqueous solution, TiO_2 nanocrystal in PC showed a higher urea yield, which is attributed by that the solvent improve the dissociation of $LiNO_3$ and make NH_3 formation easily, thereby facilitating urea synthesis. These results indicated that improving photo-generated electron-hole pairs separation and the dispersed solutions of the catalyst can enhance the performance of the photocatalytic urea synthesis.

Shchukin et al. was further used the perfluorocarbon-in-water (PFD-in-water) emulsions to stabilize and disperse the bare nano TiO_2 and Cu-

modified nano TiO_2 [107]. Through coupling the photocatalytic CO_2 and NO_3^- co-reduction reaction with the photooxidation reaction of $CHCl_3$, Cu-modified nano TiO_2 showed a higher activity for urea formation than bare TiO_2, and PFD-in-water emulsions improved the activity of urea synthesis at least two-fold for both the bare nano TiO_2 and Cu-modified nano TiO_2, attributed that the high concentration of CO_2 in the oleic phase contacting with photocatalyst is a favorable conditions for stabilizing of the reaction intermediates in case of three-phase reaction medium [107]. Subsequently, polyelectrolyte capsule was used to confine the dispersed TiO_2 nanoparticles and increase the probability of radical encounter and multielectron reduction process due to confined geometry [84]. The size effect of poly(styrene sulfonate)/poly(allylamine hydrochloride) (PVA-PAH/PSS) capsules confined Cu-modified TiO_2 nanoparticles was further investigated for urea photosynthesis from CO_2 and NO_3^- in an aqueous solution [84]. The size decrease of the confined microvolume of polyelectrolyte capsules can accelerate the NO_3^- photoreduction and increase the efficiency of urea production due to the interaction between the intermediates of the NO_3^- reduction to NH_4^+ and CO^- ion radical [84]. They obtained the highest yield of urea photosynthesis (37%) using Cu-modified TiO_2 nanoparticles encapsulated inside the 2.2 μm PVA-PAH/PSS capsules. The kind of polyelectrolyte capsules can act as one of the promising spatially confined photocatalytic reactors, to improve the utilization of light incident due to reflection and refraction in microreactor and decrease the agglomerate of photocatalyst powder.

Latterly, Kumari et al. prepared the TiO_2 (P25) and Fe-titanate supported on zeolite (HZSM-5) via sol-gel and solid-state dispersion methods [17], including Fe_2TiO_5 and Fe_2TiO_7/HZSM-5. In this study, three kinds of photocatalysts were used to urea photosynthesis from NO_3^- and isopropanol/oxalic acid in aqueous solution. In contrast to the bare P25, Fe_2TiO_5 and Fe_2TiO_7 as photocatalysts, HZSM-5 as substrates to load these catalysts can increase notably the urea yield, attributed to the improvement of charge separation on the P25, Fe_2TiO_5 and Fe_2TiO_7 loaded on HZSM-5. Fe_2TiO_5 (10 wt%)/HZSM-5 showed the maximum of 18 ppm of urea in the containing 1% isopropanol aqueous solution when achieving 90% reduction of NO_3^- to NH_3.

Although the above these studies show the activity of urea synthesis from CO_2 and NO_2^-/NO_3^-/NO, unfortunately, the light absorption of the current developed TiO_2-based photocatalysts focus mainly on the range of ultraviolet. The improvement strategies of the photo generated charge carrier are generally through Cu-doping, the size effect of TiO_2 [107], and constructing composite compound [17].

4. Summary and outlook

In this review, on the basis of that the activation energy differences of carbon and nitrogen reactants is a key factor for each pathway of urea photo/electrosynthesis, the status and challenge of the photo/electrocatalytic urea synthesis are introduced systematically from the perspective of the mechanism and photo/electrocatalysts development. Firstly, the standard reduction potential of the four kinds reaction pathways for urea photo/electrosynthesis, the possible parallel reactions, and the competitive reactions are summarized. Then, the mechanism of photo/electrocatalytic urea synthesis is introduced logically, including the key intermediates of the electrocatalytic C−N coupling and the inherent challenges on the photocatalytic urea synthesis. Lastly, both electro/photocatalysts development and those structure features are systematically compared and summarized. including the construction strategies and performance of electrocatalysts, electronic structure of active sites, the regulation strategies of the micro-environment for photocatalytic system, and the size effect and construction strategies of TiO_2-based photocatalysts. In all, photo/electrocatalytic urea synthesis via CO_2 coupling with nitrogenous small molecules has been developed to a certain stage, it still needs continuously to devote into the improvement of photo/electrocatalysts and the mechanism resolution. Several challenges and priority research opportunities need to be explored as follow：.

Primarily, both *NCON* and *NCON as the key intermediates need further to be directly revealed for the pathway of N_2 and CO_2 co-reduction. Particularly, the adsorption configuration of N_2 via side-on. Although the low adsorption energy of N_2 on catalytic sites is via side-on, the kinetic barrier of this kind N_2 adsorption configuration is still negligible because the adsorption configuration of N_2 via end-on is thermodynamically more favorable [38,109].

Secondarily, how to balance the co-adsorption, activation and coupling processes of multiple reactants through construct the component and structure of the catalyst? For examples, the Cl-coordinated Zn-Mn sites can elongate N≡N instead of break N≡N and bear the CO species [70], and the activation energy differences of CO_2 and NO_3^-/NO_2^-/NO is largely. Therefore, this challenges for the development of catalyst need to been resolved further.

Thirdly, the tuning strategies of the microenvironment at the catalytic interface should be further explored. For examples, the pH effect for the formation pathway of the key intermediate was revealed [81], and the dielectric and hydrophobic effect of the dispersed solvent was studied in photocatalytic urea synthesis process [107].

Fourthly, the visible-light-response photocatalysts and the feasible photocatalytic urea synthesis system should be further developed. Currently, the developed TiO_2-based photocatalysts mainly response to ultraviolet region [48]. The inherently contradiction between more visible light absorption and the thermodynamic feasibility of urea photosynthesis is largely challenge due to a relatively high potential of the CO_2RR to form *CO or CO. Besides, the construction strategy and disperse solution of photocatalyst need to further developed.

Finally, some novel reaction pathways should be considered to couple with photo/electrocatalytic urea synthesis. For instance, NO_3^-/NO_2^-/NO_x could be obtained by N_2 electrooxidation and the plasma-assisted oxidation [108,109], and photocatalytic urea synthesis system can be firstly photooxidation N_2 to NO_x/NO_3^-/NO_2^- and then coupling with CO_2 photoreduction to urea.

In a word, on one hand, we hope that this review inspires larger interests in developing alternative photo/electrocatalytic urea synthesis that unlock more urea formation mechanisms, further develop innovative material engineering and modification strategies to optimize the catalyst scope and improve the interfacial microenvironment. On the other hand, we believe that a blueprint for photo/electrochemical urea industrial production will be fulfilled with the persistence and unremitting efforts of scientists. Finally, photo/electrochemical urea synthesis technologies can be environmentally friendly, sustainably, recycling carbon-footprint, and distributed urea industrial production.

Declaration of Competing Interest

The authors declare that they have no known competing financial interests or personal relationships that could have appeared to influence the work reported in this paper.

Data availability

Data will be made available on request.

Acknowledgments

This work was financially supported by Guizhou Provincial Basic Research Program (Natural Science) ZK[2023]47, Innovation and Entrepreneurship Project for overseas Talents in Guizhou Province [2022]02, Specific Natural Science Foundation of Guizhou University (X202207), and Science and Technology Department of Guizhou Province (Grant No. Platform & Talents [2016]5652; [2019]5607).

Appendix A. Supporting information

Supplementary data associated with this article can be found in the online version at doi:10.1016/j.apcatb.2023.123146.

References

[1] F. Wöhler, Ueber künstliche Bildung des Harnstoffs, Ann. der Phys. 88 (1828) 253–256.
[2] A. Basarov, Direkte Darstellung des Harnstoffs aus Kohlensäure und Ammoniak, J. Pract. Chem. 2 (1868) 283.
[3] J. Meessen, Urea synthesis, Chem. Ing. Tech. 86 (2014) 2180–2189.
[4] B.M. Comer, P. Fuentes, C.O. Dimkpa, Y.-H. Liu, C.A. Fernandez, P. Arora, M. Realff, U. Singh, M.C. Hatzell, A.J. Medford, Prospects and challenges for solar fertilizers, Joule 3 (2019) 1578–1605.
[5] Y. Liu, X. Zhao, L. Ye, A novel elastic urea–melamine–formaldehyde foam: structure and properties, Ind. Eng. Chem. Res. 55 (2016) 8743–8750.
[6] L. Celleno, Topical urea in skincare: A review, Dermatol. Ther. 31 (2018), e12690.
[7] H.-M. Huang, J.J.W. McDouall, D.J. Procter, Radical anions from urea-type carbonyls: radical cyclizations and cyclization cascades, Angew. Chem. Int. Ed. 57 (2018) 4995–4999.
[8] M. Seneque, F. Can, D. Duprez, X. Courtois, NOx Selective Catalytic Reduction (NOx-SCR) by Urea: Evidence of the Reactivity of HNCO, Including a Specific Reaction Pathway for NOx Reduction Involving NO + NO_2, ACS Catal. 6 (2016) 4064–4067.
[9] Ö. Yildirim, K. Nölker, K. Büker, R. Kleinschmidt, Chemical conversion of steel mill gases to urea: an analysis of plant capacity, Chem. Ing. Tech. 90 (2018) 1529–1535.
[10] T. Kempka, M.-L. Plötz, R. Schlüter, J. Hamann, S.A. Deowan, R. Azzam, Carbon dioxide utilisation for carbamide production by application of the coupled UCG-urea process, Energy Proced. 4 (2011) 2200–2205.
[11] M. Xia, C. Mao, A. Gu, A.A. Tountas, C. Qiu, T.E. Wood, Y.F. Li, U. Ulmer, Y. Xu, C.J. Viasus, J. Ye, C. Qian, G. Ozin, Solar Urea: Towards a Sustainable Fertilizer Industry, Angew. Chem. Int. Ed. 61 (2022), e202110158.
[12] S. Liu, M. Wang, Q. Cheng, Y. He, J. Ni, J. Liu, C. Yan, T. Qian, Turning Waste into Wealth: Sustainable Production of High-Value-Added Chemicals from Catalytic Coupling of Carbon Dioxide and Nitrogenous Small Molecules, ACS Nano 16 (2022) 17911–17930.
[13] J.G. Chen, R.M. Crooks, L.C. Seefeldt, K.L. Bren, R.M. Bullock, M.Y. Darensbourg, P.L. Holland, B. Hoffman, M.J. Janik, A.K. Jones, M.G. Kanatzidis, P. King, K. M. Lancaster, S.V. Lymar, P. Pfromm, W.F. Schneider, R.R. Schrock, Beyond fossil fuel–driven nitrogen transformations, Science 360 (2018), eaar6611, https://doi.org/10.1126/science.aar6611.
[14] C. Chen, N. He, S. Wang, Electrocatalytic C–N coupling for urea synthesis, Small Sci. 1 (2021) 2100070, https://doi.org/10.1002/smsc.202100070.
[15] J.E. Kim, S. Choi, M. Balamurugan, J.H. Jang, K.T. Nam, Electrochemical C–N Bond Formation for Sustainable Amine Synthesis, Trends Chem. 2 (2020) 1004–1019.
[16] F. Matamala-Troncoso, M. Isaacs, C. Sáez-Navarrete, Photocatalyzed Production of Urea as a Hydrogen-Storage Material by TiO_2-Based Materials, Photochem 2 (2022) 539–562.
[17] B. Srinivas, V.D. Kumari, G. Sadanandam, C. Hymavathi, M. Subrahmanyam, B. R. De, Photocatalytic Synthesis of Urea from in situ Generated Ammonia and Carbon Dioxide, Photochem. Photobio. 88 (2012) 233–241.
[18] K.Y. Masami Shibata, Nagakazu Furuya, Electrochemical synthesis of urea on reduction of carbon dioxide with nitrate and nitrite ions using Cu-loaded gas-diffusion electrode, J. Electroanal. Chem. 387 (1995) 143–145.
[19] M. Jiang, M. Zhu, M. Wang, Y. He, X. Luo, C. Wu, L. Zhang, Z. Jin, Review on electrocatalytic coreduction of carbon dioxide and nitrogenous species for urea synthesis, ACS Nano 17 (2023) 3209–3224.
[20] Z. Zhang, X. Huang, B. Zhang, Y. Bi, High-performance and stable $BiVO_4$ photoanodes for solar water splitting via phosphorus–oxygen bonded FeNi catalysts, Energy Environ. Sci. 15 (2022) 2867–2873.
[21] Y. Zhang, H. Lv, Z. Zhang, L. Wang, X. Wu, H. Xu, Stable unbiased photo-electrochemical overall water splitting exceeding 3% efficiency via covalent triazine framework/metal oxide hybrid photoelectrodes, Adv. Mater. 33 (2021) 2008264.
[22] T. Banerjee, F. Podjaski, J. Kröger, B.P. Biswal, B.V. Lotsch, Polymer photocatalysts for solar-to-chemical energy conversion, Nat. Rev. Mater. 6 (2021) 168–190.
[23] C. Gao, J. Low, R. Long, T. Kong, J. Zhu, Y. Xiong, Heterogeneous Single-Atom Photocatalysts: Fundamentals and Applications, Chem. Rev. 120 (2020) 12175–12216.
[24] X. Zhang, X. Zhu, S. Bo, C. Chen, M. Qiu, X. Wei, N. He, C. Xie, W. Chen, J. Zheng, P. Chen, S.P. Jiang, Y. Li, Q. Liu, S. Wang, Identifying and tailoring C–N coupling site for efficient urea synthesis over diatomic Fe–Ni catalyst, Nat. Commun. 13 (2022) 5337.
[25] N. Meng, X. Ma, C. Wang, Y. Wang, R. Yang, J. Shao, Y. Huang, Y. Xu, B. Zhang, Y. Yu, Oxide-Derived Core–Shell Cu@Zn Nanowires for Urea Electrosynthesis from Carbon Dioxide and Nitrate in Water, ACS Nano 16 (2022) 9095–9104.
[26] M. Yuan, J. Chen, Y. Xu, R. Liu, T. Zhao, J. Zhang, Z. Ren, Z. Liu, C. Streb, H. He, C. Yang, S. Zhang, G. Zhang, Highly selective electroreduction of N_2 and CO_2 to urea over artificial frustrated Lewis pairs, Energy Environ. Sci. 14 (2021) 6605–6615.
[27] Y. Huang, R. Yang, C. Wang, N. Meng, Y. Shi, Y. Yu, B. Zhang, Direct electrosynthesis of urea from carbon dioxide and nitric oxide, ACS Energy Lett. 7 (2022) 284–291.
[28] D. Zhang, Y. Xue, X. Zheng, C. Zhang, Y. Li, Multi-heterointerfaces for selective and efficient urea production, Nat. Sci. Rev. (2022), nwac209.
[29] W. Wu, Y. Yang, Y. Wang, T. Lu, Q. Dong, J. Zhao, J. Niu, Q. Liu, Z. Hao, S. Song, Boosting electrosynthesis of urea from N_2 and CO_2 by defective Cu-Bi, Chem. Catal. 2 (2022) 3225–3238.
[30] L. Pan, J. Wang, F. Lu, Q. Liu, Y. Gao, Y. Wang, J. Jiang, C. Sun, J. Wang, X. Wang, Single-Atom or Dual-Atom in TiO_2 Nanosheet: Which is the Better Choice for Electrocatalytic Urea Synthesis? Angew. Chem. Int. Ed. 62 (2023), e202216835.
[31] K.A. Brown, D.F. Harris, M.B. Wilker, A. Rasmussen, N. Khadka, H. Hamby, S. Keable, G. Dukovic, J.W. Peters, L.C. Seefeldt, P.W. King, Light-driven dinitrogen reduction catalyzed by a CdS:nitrogenase MoFe protein biohybrid, Science 352 (2016) 448–450.
[32] H.B. Yang, S.-F. Hung, S. Liu, K. Yuan, S. Miao, L. Zhang, X. Huang, H.-Y. Wang, W. Cai, R. Chen, J. Gao, X. Yang, W. Chen, Y. Huang, H.M. Chen, C.M. Li, T. Zhang, B. Liu, Atomically dispersed Ni(i) as the active site for electrochemical CO_2 reduction, Nat. Energy 3 (2018) 140–147.
[33] Y. Wang, C. Wang, M. Li, Y. Yu, B. Zhang, Nitrate electroreduction: mechanism insight, in situ characterization, performance evaluation, and challenges, Chem. Soc. Rev. 50 (2021) 6720–6733.
[34] I. Katsounaros, On the assessment of electrocatalysts for nitrate reduction, Curr. Opin. Electrochem. 28 (2021), 100721.
[35] M.J. Liu, J. Guo, A.S. Hoffman, J.H. Stenlid, M.T. Tang, E.R. Corson, K.H. Stone, F. Abild-Pedersen, S.R. Bare, W.A. Tarpeh, Catalytic performance and near-surface X-ray characterization of titanium hydride electrodes for the electrochemical nitrate reduction reaction, J. Am. Chem. Soc. 144 (2022) 5739–5744.
[36] H. Xu, Y. Ma, J. Chen, W.-x Zhang, J. Yang, Electrocatalytic reduction of nitrate – a step towards a sustainable nitrogen cycle, Chem. Soc. Rev. 51 (2022) 2710–2758.
[37] N. Zhang, J. Shang, X. Deng, L. Cai, R. Long, Y. Xiong, Y. Chai, Governing interlayer strain in bismuth nanocrystals for efficient ammonia electrosynthesis from nitrate reduction, ACS Nano 16 (2022) 4795–4804.
[38] L. Hu, Z. Xing, X. Feng, Understanding the electrocatalytic interface for ambient ammonia synthesis, ACS Energy Lett. 5 (2020) 430–436.
[39] R. Shi, L. Shang, T. Zhang, Three Phase Interface Engineering for advanced catalytic applications, ACS Appl. Energy Mater. 4 (2021) 1045–1052.
[40] H. Jiang, R. Luo, Y. Li, W. Chen, Recent advances in solid–liquid–gas three-phase interfaces in electrocatalysis for energy conversion and storage, EcoMat 4 (2022), e12199.
[41] H. Rabiee, L. Ge, X. Zhang, S. Hu, M. Li, Z. Yuan, Gas diffusion electrodes (GDEs) for electrochemical reduction of carbon dioxide, carbon monoxide, and dinitrogen to value-added products: a review, Energy Environ. Sci. 14 (2021) 1959–2008.
[42] R. Zhang, S. Zhang, Y. Guo, C. Li, J. Liu, Z. Huang, Y. Zhao, Y. Li, C. Zhi, A Zn–nitrite battery as an energy-output electrocatalytic system for high-efficiency ammonia synthesis using carbon-doped cobalt oxide nanotubes, Energy Environ. Sci. 15 (2022) 3024–3032.
[43] Z. Sun, T. Ma, H. Tao, Q. Fan, B. Han, Fundamentals and challenges of electrochemical CO_2 reduction using two-dimensional materials, Chem 3 (2017) 560–587.
[44] Z. Tao, C.L. Rooney, Y. Liang, H. Wang, Accessing Organonitrogen Compounds via C–N Coupling in Electrocatalytic CO_2 Reduction, J. Am. Chem. Soc. 143 (2021) 19630–19642.
[45] J. Fu, Y. Yang, J.-S. Hu, Dual-Sites Tandem Catalysts for C–N Bond Formation via Electrocatalytic Coupling of CO_2 and Nitrogenous Small Molecules, ACS Mater. Lett. 3 (2021) 1468–1476.
[46] C. Chen, X. Zhu, X. Wen, Y. Zhou, L. Zhou, H. Li, L. Tao, Q. Li, S. Du, T. Liu, D. Yan, C. Xie, Y. Zou, Y. Wang, R. Chen, J. Huo, Y. Li, J. Cheng, H. Su, X. Zhao, W. Cheng, Q. Liu, H. Lin, J. Luo, J. Chen, M. Dong, K. Cheng, C. Li, S. Wang, Coupling N_2 and CO_2 in H_2O to synthesize urea under ambient conditions, Nat. Chem. 12 (2020) 717–724.
[47] Y. Huang, Y. Wang, Y. Wu, Y. Yu, B. Zhang, Electrocatalytic construction of the C-N bond from the derivates of CO_2 and N_2, Sci. China Chem. 65 (2022) 204–206.
[48] D. Li, Y. Zhao, Y. Miao, C. Zhou, L.P. Zhang, L.Z. Wu, T. Zhang, Accelerating Electron-Transfer Dynamics by TiO_2-Immobilized Reversible Single-Atom Copper for Enhanced Artificial Photosynthesis of Urea, Adv. Mater. 34 (2022), e2207793.
[49] X. Peng, L. Zeng, D. Wang, Z. Liu, Y. Li, Z. Li, B. Yang, L. Lei, L. Dai, Y. Hou, Electrochemical C-N coupling of CO_2 and nitrogenous small molecules for the electrosynthesis of organonitrogen compounds, Chem. Soc. Rev. 52 (2023) 2193–2237.
[50] Y. Ding, L. Huang, J. Zhang, A. Guan, Q. Wang, L. Qian, L. Zhang, G. Zheng, Ru-doped, oxygen-vacancy-containing CeO_2 nanorods toward N_2 electroreduction, J. Mater. Chem. A 8 (2020) 7229–7234.
[51] N. Zhang, A. Jalil, D. Wu, S. Chen, Y. Liu, C. Gao, W. Ye, Z. Qi, H. Ju, C. Wang, X. Wu, L. Song, J. Zhu, Y. Xiong, Refining Defect States in $W_{18}O_{49}$ by Mo Doping: A Strategy for Tuning N_2 Activation towards Solar-Driven Nitrogen Fixation, J. Am. Chem. Soc. 140 (2018) 9434–9443.
[52] Y. Jiang, X. Wang, D. Duan, C. He, J. Ma, W. Zhang, H. Liu, R. Long, Z. Li, T. Kong, X.J. Loh, L. Song, E. Ye, Y. Xiong, Structural Reconstruction of Cu_2O

Superparticles toward Electrocatalytic CO_2 Reduction with High C^{2+} Products Selectivity, Adv. Sci. 9 (2022) 2105292.
[53] M. Yuan, J. Chen, Y. Bai, Z. Liu, J. Zhang, T. Zhao, Q. Shi, S. Li, X. Wang, G. Zhang, Electrochemical C–N coupling with perovskite hybrids toward efficient urea synthesis, Chem. Sci. 12 (2021) 6048–6058.
[54] M. Yuan, J. Chen, H. Zhang, Q. Li, L. Zhou, C. Yang, R. Liu, Z. Liu, S. Zhang, G. Zhang, Host–guest molecular interaction promoted urea electrosynthesis over a precisely designed conductive metal–organic framework, Energy Environ. Sci. 15 (2022) 2084–2095.
[55] S. Chen, T. Takata, K. Domen, Particulate photocatalysts for overall water splitting, Nat. Rev. Mater. 2 (2017) 17050.
[56] X. Li, J. Yu, M. Jaroniec, X. Chen, Cocatalysts for selective photoreduction of CO_2 into solar fuels, Chem. Rev. 119 (2019) 3962–4179.
[57] R. Yang, Y. Fan, y Zhang, l Mei, R. Zhu, J. Qin, J. hu, Z. Chen, Y.H. Ng, D. Voiry, S. Li, Q. Lu, q wang, J.C. Yu, Z. Zeng, 2D Transition metal dichalcogenides for photocatalysis, Angew. Chem. Int. Ed. 135 (2023), e202218016.
[58] X. Li, J. Yu, M. Jaroniec, Hierarchical photocatalysts, Chem. Soc. Rev. 45 (2016) 2603–2636.
[59] X. Li, J. Wen, J. Low, Y. Fang, J. Yu, Design and fabrication of semiconductor photocatalyst for photocatalytic reduction of CO_2 to solar fuel, Sci. China Mater. 57 (2014) 70–100.
[60] G. Liu, C. Zhen, Y. Kang, L. Wang, H.-M. Cheng, Unique physicochemical properties of two-dimensional light absorbers facilitating photocatalysis, Chem. Soc. Rev. 47 (2018) 6410–6444.
[61] D.B. Kayan, F. Köleli, Simultaneous electrocatalytic reduction of dinitrogen and carbon dioxide on conducting polymer electrodes, Appl. Catal. B-Environ. 181 (2016) 88–93.
[62] H. Duan, J.-C. Liu, M. Xu, Y. Zhao, X.-L. Ma, J. Dong, X. Zheng, J. Zheng, C. S. Allen, M. Danaie, Y.-K. Peng, T. Issariyakul, D. Chen, A.I. Kirkland, J.-C. Buffet, J. Li, S.C.E. Tsang, D. O'Hare, Molecular nitrogen promotes catalytic hydrodeoxygenation, Nat. Catal. 2 (2019) 1078–1087.
[63] X. Zhu, X. Zhou, Y. Jing, Y. Li, Electrochemical synthesis of urea on MBenes, Nat. Commun. 12 (2021) 4080.
[64] J.T. Feaster, C. Shi, E.R. Cave, T. Hatsukade, D.N. Abram, K.P. Kuhl, C. Hahn, J. K. Nørskov, T.F. Jaramillo, Understanding Selectivity for the Electrochemical Reduction of Carbon Dioxide to Formic Acid and Carbon Monoxide on Metal Electrodes, ACS Catal. 7 (2017) 4822–4827.
[65] T. Cheng, H. Xiao, W.A. Goddard III, Reaction Mechanisms for the Electrochemical Reduction of CO_2 to CO and Formate on the Cu(100) Surface at 298 K from Quantum Mechanics Free Energy Calculations with Explicit Water, J. Am. Chem. Soc. 138 (2016) 13802–13805.
[66] M. Yuan, J. Chen, Y. Bai, Z. Liu, J. Zhang, T. Zhao, Q. Wang, S. Li, H. He, G. Zhang, Unveiling Electrochemical Urea Synthesis by Co-Activation of CO_2 and N_2 with Mott–Schottky Heterostructure Catalysts, Angew. Chem. Int. Ed. 60 (2021) 10910–10918.
[67] T.A. Rokob, I. Bakó, A. Stirling, A. Hamza, I. Pápai, Reactivity models of hydrogen activation by frustrated lewis pairs: synergistic electron transfers or polarization by electric field? J. Am. Chem. Soc. 135 (2013) 4425–4437.
[68] F. Barzagli, F. Mani, M. Peruzzini, From greenhouse gas to feedstock: formation of ammonium carbamate from CO_2 and NH_3 in organic solvents and its catalytic conversion into urea under mild conditions, Green. Chem. 13 (2011) 1267–1274.
[69] J. Mukherjee, S. Paul, A. Adalder, S. Kapse, R. Thapa, S. Mandal, B. Ghorai, S. Sarkar, U.K. Ghorai, Understanding the Site-Selective Electrocatalytic Co-Reduction Mechanism for Green Urea Synthesis Using Copper Phthalocyanine Nanotubes, Adv. Func. Mater. 32 (2022) 2200882.
[70] X. Zhang, X. Zhu, S. Bo, C. Chen, K. Cheng, J. Zheng, S. Li, X. Tu, W. Chen, C. Xie, X. Wei, D. Wang, Y. Liu, P. Chen, S.P. Jiang, Y. Li, Q. Liu, C. Li, S. Wang, Electrocatalytic Urea Synthesis with 63.5% Faradaic Efficiency and 100% N-Selectivity via One-step C-N coupling, Angew. Chem. Int. Ed. (2023), e202305447.
[71] H. Maimaiti, B. Xu, J.-y Sun, L.-r Feng, Photocatalytic Synthesis of Urea (CO_2/N_2/H_2O) on Coal-Based Carbon Nanotubes with the Fe-Core-Supported Ti^{3+}-TiO_2 Composite Catalyst, ACS Sustain. Chem. Eng. 9 (2021) 6991–7002.
[72] H. Liang, X. Song, Y. Zhang, Y. Wu, B. Zhao, Y. Liu, Y. Jin, L. Sheng, M. Zhao, J. Liu, Z. Li, Insight into the intrinsic driving force of NiCoP/$ZnIn_2S_{4-x}$ boosting solar urea synthesis and hydrogen production, J. Alloy. Com. 934 (2023), 167884.
[73] X. Liu, P.V. Kumar, Q. Chen, L. Zhao, F. Ye, X. Ma, D. Liu, X. Chen, L. Dai, C. Hu, Carbon nanotubes with fluorine-rich surface as metal-free electrocatalyst for effective synthesis of urea from nitrate and CO_2, Appl. Catal. B-Environ. 316 (2022), 121618.
[74] Y. Feng, H. Yang, Y. Zhang, X. Huang, L. Li, T. Cheng, Q. Shao, Te-Doped Pd Nanocrystal for Electrochemical Urea Production by Efficiently Coupling Carbon Dioxide Reduction with Nitrite Reduction, Nano Lett. 20 (2020) 8282–8289.
[75] N. Cao, Y. Quan, A. Guan, C. Yang, Y. Ji, L. Zhang, G. Zheng, Oxygen vacancies enhanced cooperative electrocatalytic reduction of carbon dioxide and nitrite ions to urea, J. Colloid Interf. Sci. 577 (2020) 109–114.
[76] J. Leverett, T. Tran-Phu, J.A. Yuwono, P. Kumar, C. Kim, Q. Zhai, C. Han, J. Qu, J. Cairney, A.N. Simonov, R.K. Hocking, L. Dai, R. Daiyan, R. Amal, Tuning the Coordination Structure of Cu–N–C Single Atom Catalysts for Simultaneous Electrochemical Reduction of CO_2 and NO_3^- to Urea, Adv. Energy Mater. 12 (2022) 2201500.
[77] C. Lv, L. Zhong, H. Liu, Z. Fang, C. Yan, M. Chen, Y. Kong, C. Lee, D. Liu, S. Li, J. Liu, L. Song, G. Chen, Q. Yan, G. Yu, Selective electrocatalytic synthesis of urea with nitrate and carbon dioxide, Nat. Sustain. 4 (2021) 868–876.
[78] C. Lv, C. Lee, L. Zhong, H. Liu, J. Liu, L. Yang, C. Yan, W. Yu, H.H. Hng, Z. Qi, L. Song, S. Li, K.P. Loh, Q. Yan, G. Yu, A defect engineered electrocatalyst that promotes high-efficiency urea synthesis under ambient conditions, ACS Nano 16 (2022) 8213–8222.
[79] M. Sun, G. Wu, J. Jiang, Y. Yang, A. Du, L. Dai, X. Mao, Q. Qin, Carbon-anchored molybdenum oxide nanoclusters as efficient catalysts for the electrosynthesis of ammonia and urea, Angew. Chem. Int. Ed. 62 (2023), e202301957.
[80] X. Wei, X. Wen, Y. Liu, C. Chen, C. Xie, D. Wang, M. Qiu, N. He, P. Zhou, W. Chen, J. Cheng, H. Lin, J. Jia, X.-Z. Fu, S. Wang, Oxygen Vacancy-Mediated Selective C–N Coupling toward Electrocatalytic Urea Synthesis, J. Am. Chem. Soc. 144 (2022) 11530–11535.
[81] X. Liu, Y. Jiao, Y. Zheng, M. Jaroniec, S.-Z. Qiao, Mechanism of C-N bonds formation in electrocatalytic urea production revealed by ab initio molecular dynamics simulation, Nat. Commun. 13 (2022) 5471.
[82] S. Kuwabata, H. Yamauchi, H. Yoneyama, Urea photosynthesis from inorganic carbon and nitrogen compounds using TiO_2 as photocatalyst, Langmuir 14 (1998) 1899–1904.
[83] B.-J. Liu, T. Torimoto, H. Yoneyama, Photocatalytic reduction of carbon dioxide in the presence of nitrate using TiO_2 nanocrystal photocatalyst embedded in SiO_2 matrices, J. Photochem. Photobio. A: Chem. 115 (1998) 227–230.
[84] D.G. Shchukin, H. Möhwald, Urea photosynthesis inside polyelectrolyte capsules: effect of confined media, Langmuir 21 (2005) 5582–5587.
[85] Y. Liu, X. Tu, X. Wei, D. Wang, X. Zhang, W. Chen, C. Chen, S. Wang, C-bound or O-bound surface: which one boosts electrocatalytic urea synthesis? Angew. Chem. Int. Ed. 62 (2023), e202300387.
[86] S. Zhang, J. Geng, Z. Zhao, M. Jin, W. Li, Y. Ye, K. Li, G. Wang, Y. Zhang, H. Yin, H. Zhang, H. Zhao, High-efficiency electrosynthesis of urea over bacterial cellulose regulated Pd–Cu bimetallic catalyst, EES Catal. 1 (2023) 45–53.
[87] X. Wei, Y. Liu, X. Zhu, S. Bo, L. Xiao, C. Chen, T.T.T. Nga, Y. He, M. Qiu, C. Xie, D. Wang, Q. Liu, F. Dong, C.L. Dong, X.Z. Fu, S. Wang, Dynamic Reconstitution Between Copper Single Atoms and Clusters for Electrocatalytic Urea Synthesis, Adv. Mater. 35 (2023), e2300020.
[88] L. Pan, J. Wang, F. Lu, Q. Liu, Y. Gao, Y. Wang, J. Jiang, C. Sun, J. Wang, X. Wang, Single-atom or dual-atom in TiO_2 nanosheet: which is the better choice for electrocatalytic urea synthesis? Angew. Chem. Int. Ed. 62 (2023), e202216835.
[89] C. Chen, S. Li, X. Zhu, S. Bo, K. Cheng, N. He, M. Qiu, C. Xie, D. Song, Y. Liu, W. Chen, Y. Li, Q. Liu, C. Li, S. Wang, Balancing sub-reaction activity to boost electrocatalytic urea synthesis using a metal-free electrocatalyst, Carbon Energy (2023), e345, https://doi.org/10.1002/cey2.3.
[90] X. Liu, P.V. Kumar, Q. Chen, L. Zhao, F. Ye, X. Ma, D. Liu, X. Chen, L. Dai, C. Hu, Carbon nanotubes with fluorine-rich surface as metal-free electrocatalyst for effective synthesis of urea from nitrate and CO_2, Appl. Catal. B-Environ. 316 (2022).
[91] V. Kyriakou, I. Garagounis, E. Vasileiou, A. Vourros, M. Stoukides, Progress in the electrochemical synthesis of ammonia, Catal. Today 286 (2017) 2–13.
[92] A.R. Singh, B.A. Rohr, J.A. Schwalbe, M. Cargnello, K. Chan, T.F. Jaramillo, I. Chorkendorff, J.K. Nørskov, Electrochemical ammonia synthesis—the selectivity challenge, ACS Catal. 7 (2017) 706–709.
[93] Y. Wang, Y. Zou, L. Tao, Y. Wang, G. Huang, S. Du, S. Wang, Rational design of three-phase interfaces for electrocatalysis, Nano Res 12 (2019) 2055–2066.
[94] Z. Lv, S. Zhou, L. Zhao, Z. Liu, J. Liu, W. Xu, L. Wang, J. Lai, Coactivation of Multiphase Reactants for the Electrosynthesis of Urea, Adv. Energy Mater. 2300946 (2023).
[95] S. Chu, X. Su, Coupling mechanism of N_2 and CO_2 to urea over artificial frustrated Lewis pairs, Chem. Catal. 2 (2022) 223–225.
[96] M. Yuan, H. Zhang, Y. Xu, R. Liu, R. Wang, T. Zhao, J. Zhang, Z. Liu, H. He, C. Yang, S. Zhang, G. Zhang, Artificial frustrated Lewis pairs facilitating the electrochemical N_2 and CO_2 conversion to urea, Chem. Catal. 2 (2022) 309–320.
[97] D. Jiao, Y. Dong, X. Cui, Q. Cai, C.R. Cabrera, J. Zhao, Z. Chen, Boosting the efficiency of urea synthesis via cooperative electroreduction of N_2 and CO_2 on MoP, J. Mater. Chem. A 11 (2023) 232–240.
[98] Z. Mei, Y. Zhou, W. Lv, S. Tong, X. Yang, L. Chen, N. Zhang, Recent progress in electrocatalytic urea synthesis under ambient conditions, ACS Sustain. Chem. Eng. 10 (2022) 12477–12496.
[99] P.H. van Langevelde, I. Katsounaros, M.T.M. Koper, Electrocatalytic nitrate reduction for sustainable ammonia production, Joule 5 (2021) 290–294.
[100] M. Shibata, K. Yoshida, N. Furuya, Electrochemical synthesis of urea at gas-diffusion electrodes III. simultaneous reduction of carbon dioxide and nitrite ions with various metal catalysts, J. Electrochem. Soc. 145 (1998) 595–600.
[101] D. Saravanakumar, J. Song, S. Lee, N.H. Hur, W. Shin, Electrocatalytic conversion of carbon dioxide and nitrate ions to urea by a titania–nafion composite electrode, ChemSusChem 10 (2017) 3999–4003.
[102] P. Siva, P. Prabu, M. Selvam, S. Karthik, V. Rajendran, Electrocatalytic conversion of carbon dioxide to urea on nano-$FeTiO_3$ surface, Ionics 23 (2017) 1871–1878.
[103] N. Meng, Y. Huang, Y. Liu, Y. Yu, B. Zhang, Electrosynthesis of urea from nitrite and CO_2 over oxygen vacancy-rich ZnO porous nanosheets, Cell Rep. Phy. Sci. 2 (2021), 100378.
[104] S. Liu, S. Yin, Z. Wang, Y. Xu, X. Li, L. Wang, H. Wang, AuCu nanofibers for electrosynthesis of urea from carbon dioxide and nitrite, Cell Rep. Phy. Sci. 3 (2022), 100869.
[105] J. Geng, S. Ji, M. Jin, C. Zhang, M. Xu, G. Wang, C. Liang, H. Zhang, Ambient Electrosynthesis of Urea with Nitrate and Carbon Dioxide over Iron-Based Dual-Sites, Angew. Chem. Int. Ed. 62 (2023), e202210958.
[106] S. Shin, S. Sultan, Z.-X. Chen, H. Lee, H. Choi, T.-U. Wi, C. Park, T. Kim, C. Lee, J. Jeong, H. Shin, T.-H. Kim, H. Ju, H.C. Yoon, H.-K. Song, H.-W. Lee, M.-

J. Cheng, Y. Kwon, Copper with an atomic-scale spacing for efficient electrocatalytic co-reduction of carbon dioxide and nitrate to urea, Energy Environ. Sci. 16 (2023) 2003–2013.

[107] E.A. Ustinovich, D.G. Shchukin, D.V. Sviridov, Heterogeneous photocatalysis in titania-stabilized perfluorocarbon-in-water emulsions: Urea photosynthesis and chloroform photodegradation, J. Photochem. Photobio. A: Chem.,175 (2005) 249–252.

[108] X. Zhang, R. Shi, Z. Li, J. Zhao, H. Huang, C. Zhou, T. Zhang, Photothermal-assisted photocatalytic nitrogen oxidation to nitric acid on palladium-decorated titanium oxide, Adv. Energy Mater. 12 (2022) 2103740.

[109] Y. Wang, T. Li, Y. Yu, B. Zhang, Electrochemical synthesis of nitric acid from nitrogen oxidation, Angew. Chem. Int. Ed. 61 (2022), e202115409.